HEALTH AND MEDICINE

10.1126/sciadv.1600349

Tumor-homing peptides as tools for targeted delivery of payloads to the placenta

Anna King,[1,2] Cornelia Ndifon,[1,2] Sylvia Lui,[1,2] Kate Widdows,[1,2] Venkata R. Kotamraju,[3,4] Lilach Agemy,[3,4]* Tambet Teesalu,[3,4†] Jocelyn D. Glazier,[1,2] Francesco Cellesi,[5‡] Nicola Tirelli,[5,6] John D. Aplin,[1,2] Erkki Ruoslahti,[3,4] Lynda K. Harris[1,2,5§]

The availability of therapeutics to treat pregnancy complications is severely lacking mainly because of the risk of causing harm to the fetus. As enhancement of placental growth and function can alleviate maternal symptoms and improve fetal growth in animal models, we have developed a method for targeted delivery of payloads to the placenta. We show that the tumor-homing peptide sequences CGKRK and iRGD bind selectively to the placental surface of humans and mice and do not interfere with normal development. Peptide-coated nanoparticles intravenously injected into pregnant mice accumulated within the mouse placenta, whereas control nanoparticles exhibited reduced binding and/or fetal transfer. We used targeted liposomes to efficiently deliver cargoes of carboxyfluorescein and insulin-like growth factor 2 to the mouse placenta; the latter significantly increased mean placental weight when administered to healthy animals and significantly improved fetal weight distribution in a well-characterized model of fetal growth restriction. These data provide proof of principle for targeted delivery of drugs to the placenta and provide a novel platform for the development of placenta-specific therapeutics.

INTRODUCTION

More than 10% of pregnant women develop serious complications, such as preeclampsia (PE) and fetal growth restriction (FGR) (*1*–*3*), which result in significant maternofetal morbidity and mortality. The underlying cause of these conditions is a poorly functioning placenta: Impaired placental perfusion, reduced surface area, altered cell turnover, and diminished nutrient transport capacity are all associated with impaired fetal growth (*4*, *5*) and often result in iatrogenic preterm delivery. The consequences are twofold: In the short term, premature babies are at high risk of developing respiratory distress syndrome, retinopathy, cerebral palsy, and infections. In the long term, small size at birth is associated with an increased risk of elevated cardiovascular disease, type 2 diabetes, and adiposity in adulthood (*6*). Despite this, current treatments for PE and FGR are limited to induction of labor and early delivery, leading to expensive neonatal intensive care costs and exacerbation of adverse health outcomes in affected offspring.

Potential therapeutics have been identified that enhance placental growth and function, alleviate maternal symptoms, and improve fetal growth in animal models of pregnancy complications (*7*–*9*), yet pregnant women are considered to be a high-risk, low-return cohort. As a consequence, only three new drugs have been licensed for use in pregnancy in the last 20 years, two of which are used after delivery (*10*, *11*). To address this, we have developed a method for synaphic [affinity-based (*12*)] drug targeting, as a means of focusing drug action within the placenta, while minimizing side effects in other maternal and fetal tissues. This technology was originally developed to facilitate targeted delivery of chemotherapeutics to tumors and tumor vasculature (*12*, *13*), which express cell surface antigens that are absent from healthy vessels and tissues (*13*, *14*). Tumor-specific "receptors" are available to bind circulating ligands, for example, peptides and antibodies (*15*, *16*); attaching a diagnostic or therapeutic payload to these ligands allows the payload to become concentrated in tumor tissue, thereby improving efficacy and reducing the off-target exposure of normal tissues. For example, the pentapeptide CGKRK (Cys-Gly-Lys-Arg-Lys) targets tumor neovasculature in mouse models of epidermal carcinogenesis (*17*), glioblastoma (*18*), and breast cancer (*19*), and the cyclic peptide iRGD (Cys-Arg-Gly-Asp-Lys-Gly-Pro-Asp-Cys) has been used to deliver Abraxane to tumor vessels in several xenograft models (*20*).

The villous placenta shares common physiological and biochemical features with solid tumors, including the ability to undergo rapid proliferation, to produce a variety of growth factors and cytokines, and to evade immune surveillance (*21*). Furthermore, a distinct population of extravillous trophoblast (EVT) cells displays behavior similar to that exhibited by metastatic cells: In early pregnancy, EVT cells egress from placental villi, invade the uterine wall, and remodel the uterine spiral arteries (*22*). Because the placenta behaves like a well-controlled tumor, we hypothesized that existing tumor-homing sequences would bind to antigens selectively expressed on the placental surface. Here, we demonstrate that tumor-homing peptides can be exploited for targeted delivery of payloads to the placenta in mice and humans. We envision that this technology could be clinically used to provide the first treatments

[1]Maternal and Fetal Health Research Centre, Institute of Human Development, University of Manchester, Manchester M13 9WL, UK. [2]Academic Health Science Centre, St Mary's Hospital, Oxford Road, Manchester M13 9WL, UK. [3]Cancer Center, Sanford Burnham Prebys Medical Discovery Institute, 10901 North Torrey Pines Road, La Jolla, CA 92037, USA. [4]Center for Nanomedicine and Department of Molecular Cellular and Developmental Biology, University of California, Santa Barbara, Santa Barbara, CA 93106–9610, USA. [5]School of Pharmacy, University of Manchester, Stopford Building, Oxford Road, Manchester M13 9PT, UK. [6]Institute of Inflammation and Repair, Faculty of Medical and Human Sciences, University of Manchester, Manchester M13 9PT, UK.
*Present address: Weizmann Institute of Science, 234 Herzl Street, Rehovot 76100, Haifa, Israel.
†Present address: Laboratory of Cancer Biology, Institute of Biomedicine, Centre of Excellence for Translational Medicine, University of Tartu, Ravila 14b, 50411 Tartu, Estonia.
‡Present address: Fondazione CEN-European Centre for Nanomedicine, Piazza Leonardo da Vinci 32, 20133 Milan, Italy; Fondazione IRCCS Ca' Granda Ospedale Maggiore Policlinico, Via Pace 9, I-20122 Milan, Italy; and Dipartimento di Chimica, Materiali ed Ingegneria Chimica "G. Natta," Politecnico di Milano, Via Mancinelli 7, 20131 Milan, Italy.
§Corresponding author. Email: lynda.k.harris@manchester.ac.uk

for a poorly functioning placenta while simultaneously mitigating the risks associated with administration of drugs in pregnancy.

RESULTS

Tumor-homing peptides bind to epitopes expressed at the murine maternofetal interface

To examine whether selected tumor-homing peptides could be exploited for placental targeting, we intravenously injected T7 bacteriophage displaying the surface peptide CGKRK or CRGDKGPDC (iRGD) into pregnant mice. Quantification of phage titers showed significant enrichment in placental tissue compared to other organs (Fig. 1A). Next, we synthesized the individual peptides, labeled them with 5(6)-carboxyfluorescein (FAM), and intravenously injected them into pregnant mice. Histological analysis showed that both FAM-CGKRK and FAM-iRGD bound to the labyrinth (the region of nutrient exchange) and to the decidual spiral arteries (the maternal component of the placenta), but not to the junctional zone (the endocrine component of the placenta) adjacent to the labyrinth, at multiple time points in gestation (Fig. 1, B to G). The peptides did not accumulate in the vascular beds of other major organs but were excreted via the kidney (fig. S1). The previously characterized control peptide FAM-ARALPSQRSR (FAM-ARA) did not target the maternofetal interface (Fig. 1, H to J). Immunostaining with antibodies to the trophoblast marker cytokeratin-7, the vascular endothelial marker MECA, the junctional zone marker trophoblast-specific protein α (Tpbpa), and the labyrinthine markers cathepsin Q (Ctsq) and glial cells missing (GCM-1) revealed that FAM-CGKRK colocalized with the endothelium of unremodeled decidual spiral arteries and also with endovascular trophoblast lining remodeled vessel segments (figs. S2, A and B, and S3A). FAM-iRGD showed a similar binding pattern (figs. S2, C and D, and S3E). FAM-CGKRK and FAM-iRGD also bound to vascular endothelial cells and trophoblast cells within the labyrinth (figs. S2, E and F, and S3, B, C, F, and G).

Repeated administration of CGKRK or iRGD during pregnancy does not adversely affect pregnancy outcome in mice

To determine whether peptide binding interfered with normal placental function or was affected upon reproductive outcome, we injected pregnant mice with vehicle [phosphate-buffered saline (PBS)] or peptide (100 μg per mouse) on embryonic day 11.5 (E11.5), E13.5, and E15.5. Fetuses and placentas were collected and weighed on E18.5. Intravenous administration of peptide had no effect on litter size, number of resorptions, fetal weight, placental weight, or maternal weight gain (Fig. 2); however, iRGD modestly increased fetal to placental weight ratio ($P < 0.01$; Fig. 2E). Treatment did not alter rates of proliferation or apoptosis in the mouse placenta at E18.5, as measured by Ki67 and active caspase-3 immunostaining, respectively (fig. S4).

Tumor-homing peptides accumulate within the syncytiotrophoblast layer of human placental explants

To assess whether FAM-CGKRK and FAM-iRGD bind to the surface of human placenta, we incubated explants of human first-trimester or term placental tissue with peptide for up to 24 hours. FAM-CGKRK rapidly accumulated within the outer syncytiotrophoblast (STB) layer of first-trimester placenta and was retained within the STB, rather than penetrating into the underlying cytotrophoblast (CTB) layer (Fig. 3A). Fluorescence within the villous stroma was noted occasionally but correlated with loss of the overlying STB. Following a 24-hour pulse-chase experiment, FAM-CGKRK was still evident within the STB. Similar data were obtained when FAM-CGKRK was cultured with term placental explants (Fig. 3B). Fluorescence colocalized with the trophoblast marker cytokeratin-7 (fig. S5, A and B).

Uptake of FAM-iRGD into the STB of first-trimester placenta followed different kinetics: Fluorescence was only detected after 30 min of incubation, although FAM-iRGD continued to accumulate within the STB layer after this time (Fig. 3C). Similar data were obtained when FAM-iRGD was cultured with term placental explants (Fig. 3D). Again, FAM-iRGD was only observed in the underlying tissue when the STB layer was damaged or lost, and fluorescence colocalized with cytokeratin-7 immunostaining (fig. S5, C and D). In contrast to FAM-CGKRK, minimal fluorescence was evident after 24 hours. FAM-ARA did not bind to the syncytium of human placenta or to other cellular components (Fig. 3, E and F). To ensure that peptide binding did not alter trophoblast cell turnover, we incubated human first-trimester placental explants with vehicle or peptide for up to 48 hours. Treatment with CGKRK or iRGD did not alter basal rates of CTB proliferation (Fig. 3G), but iRGD treatment modestly reduced the rate of CTB apoptosis ($P < 0.05$; Fig. 3H).

Membrane-associated calreticulin is a receptor for CGKRK

Previous studies have identified α_v integrins as the receptors for iRGD in tumors (*20*); in keeping with this, FAM-iRGD colocalized with integrin α_v in the mouse placenta (fig. S6). We also identified calreticulin as a receptor for CGKRK on the placental surface: We applied mouse placental homogenates to an affinity chromatography column containing immobilized CGKRK peptide, eluted bound proteins by adding excess CGKRK, and identified them by matrix-assisted laser desorption/ionization–time-of-flight (MALDI-TOF) mass spectrometry. The eluates contained peptide fragments from several proteins, of which calreticulin was the most abundant (Table 1). Western blotting confirmed the presence of calreticulin in the eluate (Fig. 4A). The other proteins predicted by mass spectrometry were not detected in the eluate and so were not investigated further. Calreticulin is highly expressed in the labyrinth, junctional zone, and spiral arteries of the mouse placenta (Fig. 4, B to D) and in the syncytium of human first-trimester and term placenta (Fig. 4, E to G). Moreover, FAM-CGKRK bound to recombinant human calreticulin (Fig. 4H; estimated binding affinity of $K_d = 0.59$ μM), and a 50% decrease in calreticulin mRNA expression following small interfering RNA (siRNA) treatment of term placental explants (fig. S7) correlated with a similar decrease in FAM-CGKRK binding (siRNA 1, 58.6 ± 6.9%; siRNA 2, 56.7 ± 10.3%; Fig. 4I). Calreticulin colocalized in the STB of human term placental explants with FAM-CGKRK binding sites (Fig. 4J), and localization of calreticulin to the placental microvillous membrane (MVM) was confirmed by flow cytometry of an MVM-derived vesicle preparation (Fig. 4K). FAM-CGKRK binding to MVM vesicles was reduced to 59.5 ± 3.3% of control values in the presence of recombinant human calreticulin (Fig. 4L). These data identify membrane-associated calreticulin as a placental receptor for CGKRK.

Tumor-homing peptides facilitate targeted delivery of iron oxide nanoworms to the mouse placenta

To ensure that the peptides retained their function when attached to a nanoparticle, we coated iron oxide nanoparticles [approximately 180 nm in length; dubbed nanoworms because of their elongated shape (*23*)] with FAM-CGKRK, FAM-iRGD, or FAM-ARA and intravenously injected them into pregnant mice. Nanoworms coated with FAM-CGKRK

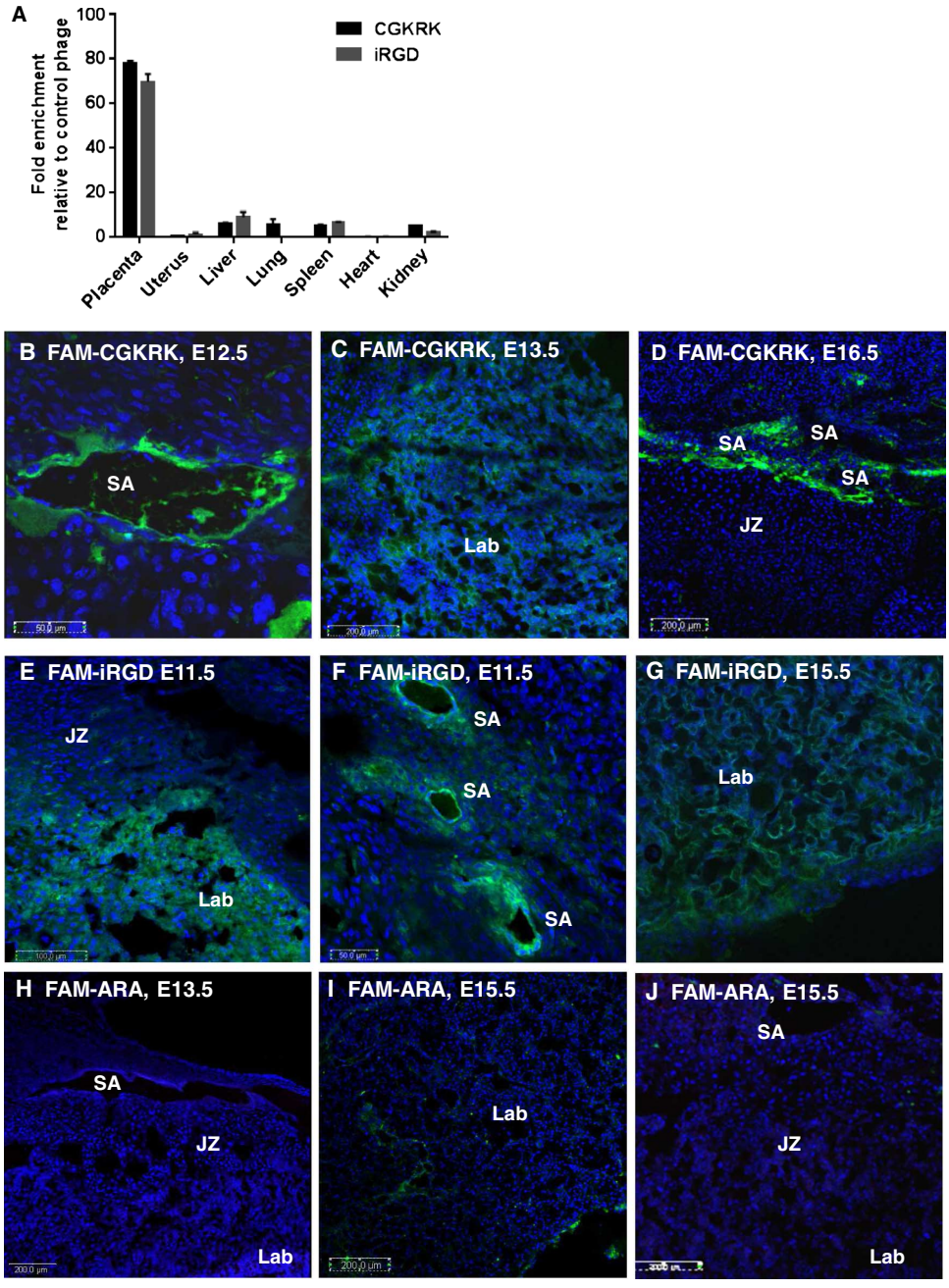

Fig. 1. Tumor-homing sequences CGKRK and iRGD target the mouse placenta. (**A**) Pregnant mice ($n = 3$ per group) were intravenously injected with phage bearing the surface peptides CGKRK or iRGD or the control sequence G7 (1.5×10^{10} colony-forming units per mouse). After 30 min, mice were subjected to cardiac perfusion; phage were recovered from individual organs and quantified; results are expressed as fold titers relative to those of the control sequence G7. (**B** to **J**) Synthetic peptides (200 μg) were injected into the tail vein of pregnant mice. After 3 hours, mice were subjected to cardiac perfusion to remove unbound peptide. Placentas were collected, fixed, and frozen; evidence of peptide binding was assessed by fluorescence microscopy. $n = 3$ placentas were examined from each of $n = 4$ pregnant mice. Representative images are shown. (B to D) FAM-CGKRK. (E to G) FAM-iRGD. (H to J) FAM-ARA (control). Green, FAM-labeled peptides; blue, 4′,6-diamidino-2-phenylindole (DAPI; nuclei). JZ, junctional zone; Lab, labyrinth; SA, spiral artery.

or FAM-iRGD accumulated at the maternofetal interface (Fig. 5, A to F), whereas nanoworms coated with the control peptide FAM-ARA did not (Fig. 5, G to I). As observed with the soluble peptides, nanoworms bound to the endothelium of the uterine spiral arteries and accumulated within the placental labyrinth. FAM-CGKRK and FAM-iRGD nanoworms were observed in some areas of the liver and spleen as previously described (*24*), but they did not accumulate in other major organs; FAM-ARA nanoworms were observed in high numbers throughout the liver and spleen (fig. S8). These data show that the targeting properties of the peptides are retained when they are attached to nanoparticles.

Tumor-homing peptides facilitate targeted delivery of peptide-decorated liposomes to the mouse placenta

To create biocompatible nanocarriers for targeted delivery of payloads to the placenta, we synthesized liposomes decorated with TAMRA-CGKRK, rhodamine-iRGD, or TAMRA-ARA (Fig. 6A; Z-average diameter: CGKRK, 156 nm; iRGD, 146 nm; and ARA, 142 nm), loaded them with the fluorescent drug analog carboxyfluorescein (CF; 100 mM), and intravenously injected them into pregnant mice. Targeted liposomes accumulated at the maternofetal interface and discrete areas of green fluorescence indicative of CF release were observed after 24 hours. CGKRK-decorated liposomes predominantly accumulated in the labyrinth, whereas iRGD-decorated liposomes were also observed within the spiral arteries (Fig. 6, B to G). With the exception of the liver and spleen, which nonselectively take up all nanoparticles (*24*), targeted liposomes were not observed in other major organs (fig. S9, A and B); pink-colored urine also indicated peptide excretion via the kidney (fig. S9C), as previously described (*18*, *24*). After 72 hours, targeted liposomes were still observed within the placenta (Fig. 6), but the amount present in maternal clearance organs was markedly reduced (fig. S10). ARA-decorated liposomes modestly accumulated in the decidua and in the labyrinth (Fig. 6, H to J), but were also observed at high levels in the maternal lung, the maternal clearance organs, and fetal tissues from 6 to 72 hours (fig. S11). The CF cargo of liposomes lacking a targeting peptide (and therefore a peptide-conjugated red fluorophore) was observed in the liver from 6 to 72 hours, the spleen at 24 hours, and the fetus from 24 to 72 hours (fig. S12).

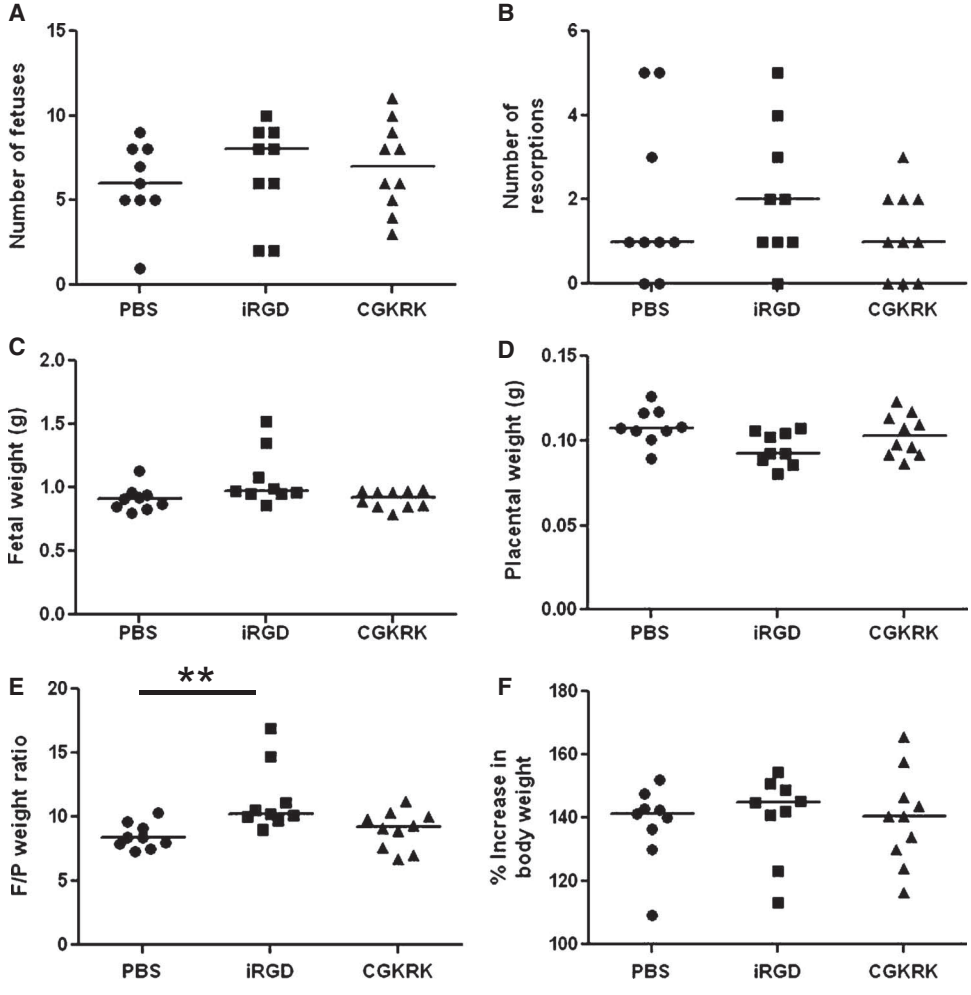

Fig. 2. Administration of tumor-homing peptides does not alter reproductive outcome. Pregnant mice were intravenously injected with PBS (100 μl), acetyl (Ac)–iRGD, or Ac-CGKRK (100 μg) at E11.5, E13.5, and E15.5. (**A** to **F**) Mice were sacrificed at E18.5, and the following variables were measured: number of fetuses per litter (A), number of resorptions per litter (B), fetal weight (C), placental weight (D), fetal/placental (F/P) weight ratio (E), and percent increase in maternal body weight from E10.5 to E18.5 (F). Data points represent mean value per litter; horizontal line represents median. $^{**}P < 0.01$, Kruskal-Wallis test. PBS ($n = 9$), iRGD ($n = 9$), CGKRK ($n = 10$).

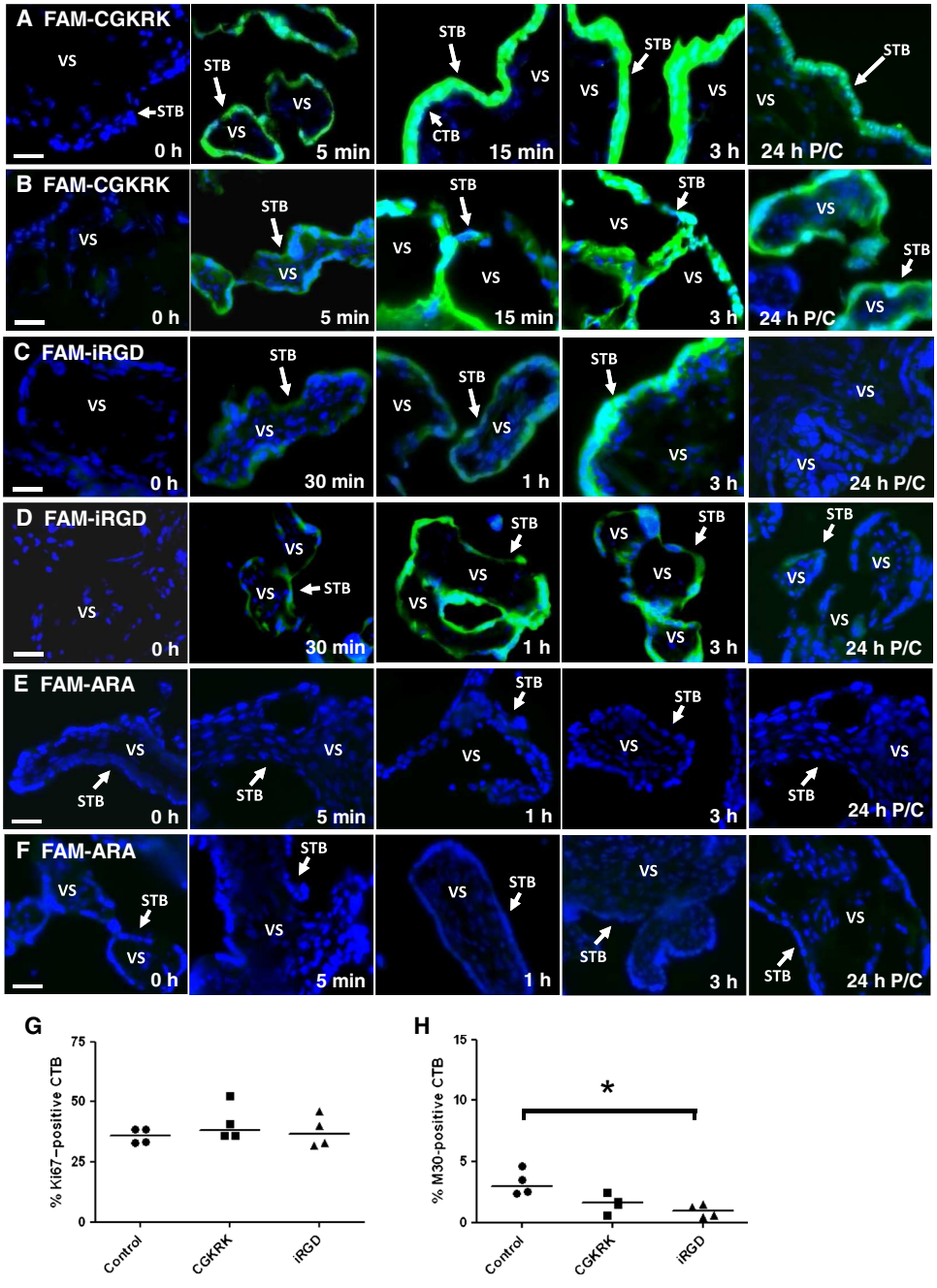

Fig. 3. Tumor-homing peptides accumulate in the syncytium of human placental explants. (**A** to **F**) First-trimester (A, C, and E) or term placental explants (B, D, and F) were incubated with peptide (20 μM) for 0 to 3 hours. For pulse-chase (P/C) experiments, explants were incubated with peptide for 3 hours, then transferred to fresh medium, and cultured for a further 21 hours. Binding and uptake were assessed by fluorescence microscopy ($n = 3$). (A and B) FAM-CGKRK. (C and D) FAM-iRGD. (E and F) FAM-ARA. Green, FAM-labeled peptides. VS, villous stroma. Scale bars, 50 μm. (**G** and **H**) First-trimester placental explants were serum-starved for 24 hours and then incubated with vehicle control (PBS), Ac-CGKRK, or Ac-iRGD (20 μM). CTB proliferation and apoptosis were quantified at 24 and 48 hours, respectively, by immunostaining for Ki67 and M30, respectively. Median ($n = 4$ placentas). *$P < 0.05$, Kruskal-Wallis test.

Table 1. Peptides identified by MALDI-TOF mass spectrometry.

Protein	Gene ID	Total number of peptides identified	Number of unique peptides identified
Calreticulin	Calr	21	4
Aspartyl aminopeptidase A	DNPEP	3	2
Proteasome subunit β type-6	PSMB6	3	2
Protein disulfide isomerase 6	Pdia6	6	2
Triosephosphate isomerase	Tpi1	3	3

We also incubated peptide-decorated liposomes with human term placental explants to examine binding and uptake in human tissue. Targeted liposomes facilitated delivery of CF to the syncytium of placental explants ex vivo; however, delivery was not achieved when ARA-decorated liposomes were used (Fig. 6, K to M).

Targeted delivery of insulin-like growth factor 2 increases placental weight in the C57BL/6J mouse

Insulin-like growth factor 2 (IGF-2) is a critical mediator of placental growth in both mice and humans (*25*, *26*), but the IGF receptors are ubiquitously expressed in maternal and fetal tissues. Thus, we selected IGF-2 as an ideal candidate therapeutic to be administered systemically via targeted liposomes. We hypothesized that targeted delivery of IGF-2 to the placenta would enhance placental growth, translating into increased placental weights at E18.5 and leading to a corresponding increase in fetal weight. Healthy pregnant mice were injected with four doses of vehicle (PBS) and systemically administered IGF-2, empty liposomes, or liposomes containing IGF-2, and fetuses and placentas were harvested on E18.5. IGF-2 administered in iRGD-decorated liposomes significantly increased placental weights compared to mice injected with empty liposomes decorated with iRGD or ARA or mice injected with PBS alone (Fig. 7A). Delivery of IGF-2 in iRGD-decorated liposomes was more effective in increasing placental weights than delivery of IGF-2 in plain or nontargeted liposomes or via intravenous injection of free IGF-2. In addition, fewer of the smaller (lighter) placentas were observed after treatment with iRGD liposomes containing IGF-2 compared to all other control groups, suggesting that growth of the smallest placentas was enhanced, whereas larger placentas were unaffected. Despite this, increased placental weight did not correlate with increased fetal weight; fetal weight was significantly increased by plain liposomes but not by any other treatment (Fig. 7B). Mean litter size and number of resorptions were not altered by any treatment, suggesting that liposomes are well tolerated in pregnancy (fig. S13, A and B); maternal kidney and spleen weights were similarly unaffected, suggesting minimal off-target accumulation of IGF-2 in the clearance organs (fig. S13, C and D). Because empty CGKRK–decorated liposomes reduced fetal weight compared to treatment with plain liposomes or PBS, this nanocarrier was not used for IGF-2 delivery (Fig. 7B).

Targeted delivery of IGF-2 improves fetal weight distribution in the P0 mouse model of FGR

Because increased placental growth did not translate into increased fetal growth in healthy wild-type mice, we tested our targeted liposomes in a mouse model of FGR, the placenta-specific (P0) *Igf-2* knockout mouse. Males heterozygous for the deletion of the P0 transcript are mated with C57BL/6J females, producing mixed litters of healthy wild-type and growth-restricted P0 pups. Placental weights of P0 pups are reduced at E12 and remain smaller throughout gestation (68% wild-type weight at E19); however, P0 fetuses are only growth-restricted in late gestation (96% wild-type weight at E16, 78% wild-type weight at E19, and 69% wild-type weight at birth) (*25*). Pregnant mice were injected with vehicle, free IGF-2, or iRGD-decorated liposomes containing IGF-2. Unlike in C57BL/6J mice, targeted delivery of IGF-2 did not significantly increase placental weight in wild-type or P0 pups (Fig. 8A). Similarly, targeted delivery of IGF-2 did not significantly increase fetal weight (Fig. 8B) or alter fetal weight distribution in wild-type pups (Fig. 8C). However, targeted liposomes containing IGF-2 significantly increased fetal weight of P0 fetuses (83% wild-type weight) and significantly altered fetal weight distribution, with fewer of the smallest (lowest weight) pups being observed (Fig. 8C), a clinically relevant outcome. Moreover, litter size and number of resorptions were unaffected by treatment (fig. S14, A and B), suggesting that the growth of the smallest P0 fetuses was enhanced, without any pregnancy losses occurring; this phenomenon has been observed in the $eNOS^{-/-}$ mouse model of FGR, following systemic administration of Leu^{27} IGF-2 (*27*). As observed in wild-type mice, maternal spleen and kidney weights were unaffected by treatment (fig. S14, C and D).

DISCUSSION

Currently, there are no therapeutics available to treat a poorly functioning placenta and alleviate the resulting maternal and fetal symptoms. Here, we demonstrate that the specific tumor-homing peptide sequences CGKRK and iRGD bind to the surface of mouse and human placental tissue and can be exploited for targeted delivery of payloads to the placenta. We observed that soluble peptides and peptide-decorated nanoparticles bound to murine decidual spiral arteries and to the vasculature of the placental labyrinth at multiple time points in gestation. CGKRK and iRGD also bound to the surface of human placental explants, acting as effective cell-penetrating peptides, which rapidly accumulate in the outer syncytial layer. Similarly, targeted liposomes were internalized by the syncytium of placental explants, and release of their CF cargo was observed. Finally, iRGD-decorated liposomes were used to selectively deliver IGF-2 to mouse placenta, resulting in enhancement of placental growth in healthy mice and an improved fetal weight distribution in growth-restricted mice. Given the current drug drought in obstetrics, a targeted therapy that promotes the growth of the smallest babies without inducing overgrowth of those that are developing optimally fulfills an important clinical need that is currently unmet.

Targeted delivery of chemotherapeutics using iron oxide nanoworms has been shown to maximize drug efficacy in tumor models (*18*). As proof-of-principle experiment, we demonstrated that peptide-decorated nanoworms effectively target the mouse placenta, although this

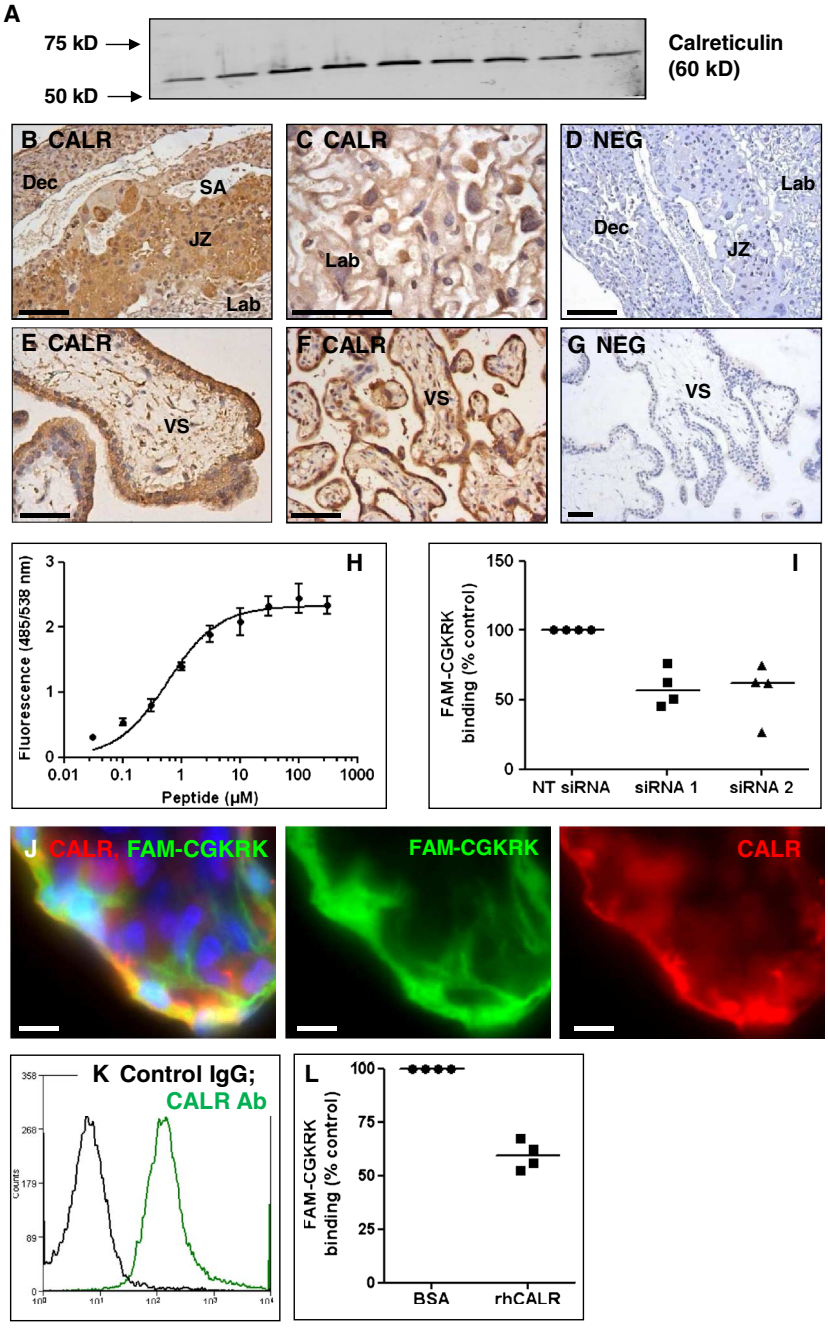

Fig. 4. CGKRK binds to membrane-associated calreticulin. Mouse placental homogenates were applied to a chromatography column containing immobilized CGKRK peptide. Bound proteins were eluted with excess CGKRK. (**A**) Immunoblot of sequential column eluent fractions. (**B** to **G**) Immunostaining of mouse placenta (B to D), human first-trimester placenta (E and G), or human term placenta (F) for calreticulin (B, C, E, and F) or control immunoglobulin G (IgG) (D and G). Dec, decidua. Scale bars, 50 μm (representative images, $n = 4$). (**H**) Affinity of CGKRK for recombinant calreticulin. Binding of increasing concentrations of FAM-CGKRK to immobilized calreticulin was measured and normalized to nonspecific peptide binding. Mean ± SEM ($n = 4$). (**I**) Human term placental explants cultured with nontargeting (NT) siRNA or calreticulin-specific siRNA sequences; following calreticulin knockdown, explants were incubated with FAM-CGKRK (20 μM; 30 min). Fluorescence of tissue supernatants was quantified. Median ($n = 4$). (**J**) Human first-trimester placenta incubated with FAM-CGKRK (20 μM; 30 min; green) and immunostained with an antibody to calreticulin (red). Blue, DAPI (nuclei). Scale bars, 10 μm; $n = 4$. (**K**) MVM vesicles labeled with calreticulin antibody (green) or control IgG (black); binding was quantified by flow cytometry (representative histogram, $n = 4$). (**L**) MVM vesicles incubated with FAM-CGKRK (20 μM) and bovine serum albumin (BSA) (control; 10 μg) or recombinant human calreticulin (10 μg) for 30 min. FAM-CGKRK binding was quantified by flow cytometry. Median ($n = 4$).

form of nanocarrier is unlikely to be compatible with optimal placental function. Systemic administration of silica or titanium oxide nanoparticles to pregnant mice has been shown to induce structural and functional changes in the placenta and impair fetal growth (*28*); thus, we created peptide-decorated liposomes as our biocompatible nanocarrier of choice. Candidate payloads would include compounds that improved placental function and enhanced pregnancy outcome by modulating cellular growth pathways, maternofetal or fetoplacental vascular physiology, or local oxidative stress, but would require tissue-specific delivery. For example, systemic administration of sildenafil citrate normalizes uteroplacental blood flow and promotes fetal growth in mouse models of PE and FGR (*9*, *29*), but also reportedly has detrimental effects in fetal vascular function (*30*). Similarly, IGF-2, a key mediator of placental growth (*25*, *26*), increases fetal and placental weights and promotes fetal survival in guinea pigs (*31*), but if freely administered, it can interact with ubiquitously expressed IGF receptors in all maternal tissues. Here, we observed enhanced placental and fetal growth in healthy mice and mice exhibiting FGR, respectively, following targeted delivery of IGF-2, demonstrating that our engineered nanoparticles are well tolerated and can elicit tissue-specific benefits in pregnancy, and that the encapsulated IGF-2 remained bioactive. Previously, we have delineated growth signaling pathways in the placenta downstream of IGF stimulation of the outer STB layer (*26*). Thus, the syncytial-specific nature of targeting we observed in human placental tissue suggests that targeted liposomes will facilitate delivery of therapeutics directly to the trophoblast, providing the opportunity to modulate its function as a means of enhancing placental efficiency and improving maternal and fetal outcomes.

In tumors, α_v integrins are the receptors for the iRGD-homing sequence (*20*); these are adhesion molecules that mediate extracellular matrix attachment and cell signaling. Integrin α_v is constitutively expressed within the mouse placenta throughout gestation (*32*), and we demonstrate here that FAM-iRGD colocalizes with integrin α_v–expressing cells at the maternofetal interface. Integrin $\alpha_v\beta_3$ is expressed on the human placental surface (*33*) and by invasive EVT cells that colonize the maternal spiral arteries (*34*). p32 has recently been identified as the main cell surface receptor for CGKRK in tumors (*19*, *35*) and is highly expressed in the

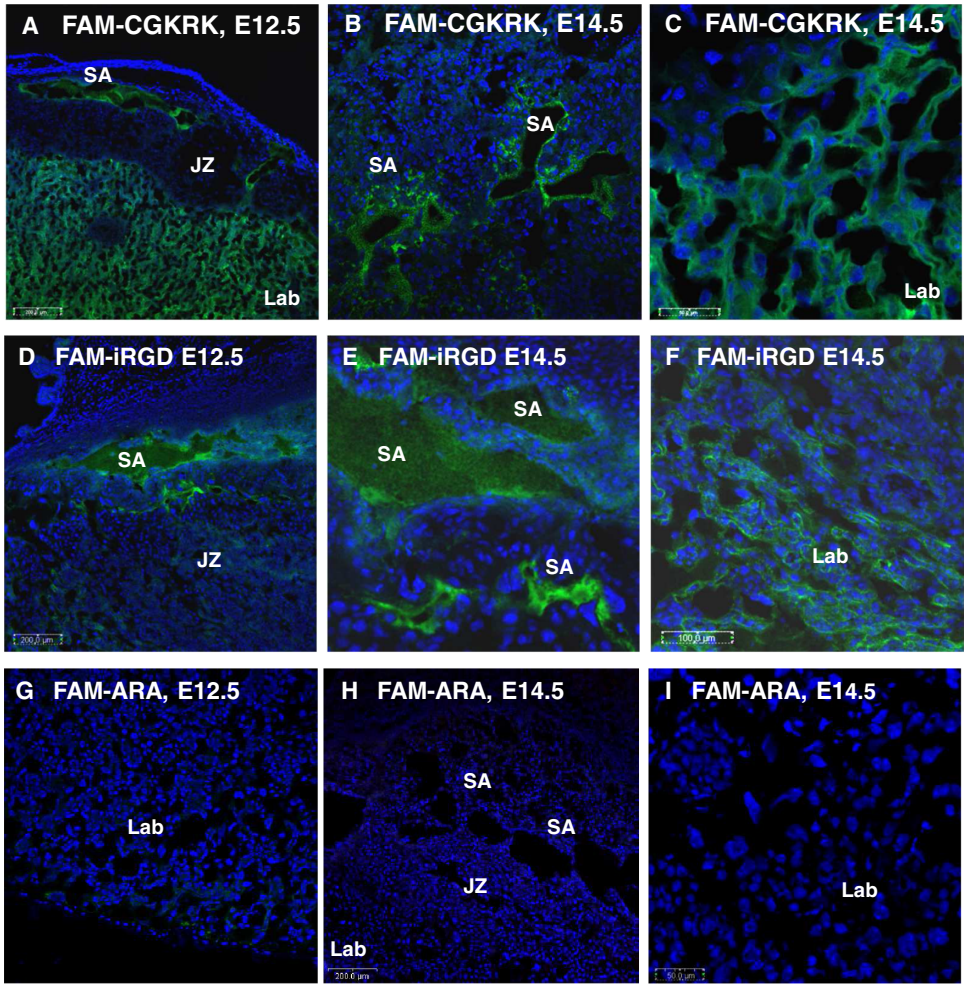

Fig. 5. Tumor-homing peptides facilitate delivery of iron oxide nanoworms to the mouse placenta. Peptide-coated iron oxide nanoworms (5 mg of iron/kg body weight) were injected into the tail vein of pregnant mice. After 3 hours, mice were subjected to cardiac perfusion to remove unbound nanoworms. Placentas were collected, fixed, and frozen; evidence of nanoworm binding was assessed by confocal microscopy. Representative images are shown. (**A** to **C**) FAM-CGKRK ($n = 3$ placentas from $n = 4$ mice). (**D** to **F**) FAM-iRGD ($n = 3$ placentas from $n = 3$ mice). (**G** to **I**) FAM-ARA ($n = 3$ placentas from $n = 3$ mice). Green, FAM-labeled nanoworms; blue, DAPI (nuclei). Scale bar, 50 μm.

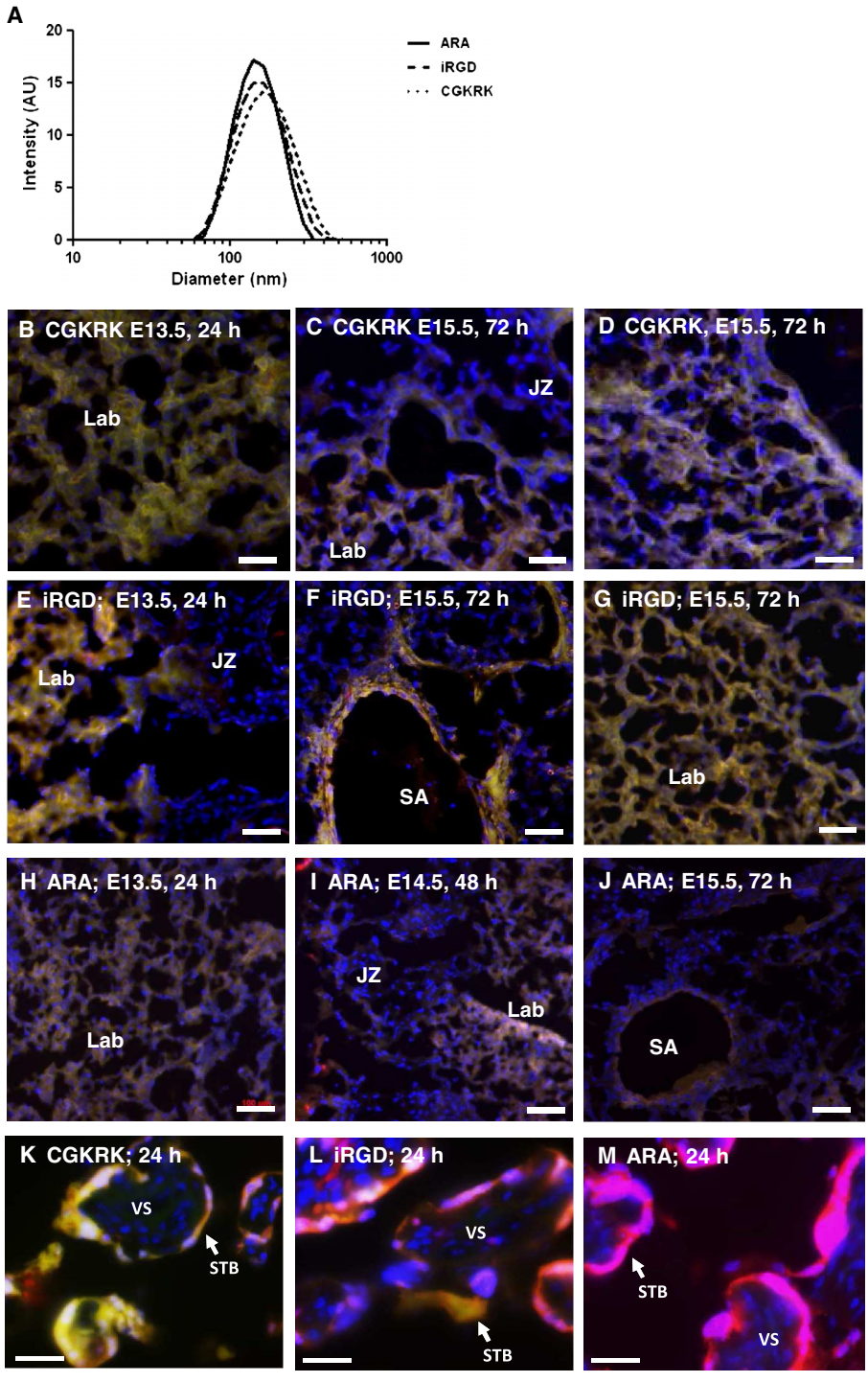

Fig. 6. Liposomes decorated with tumor-homing peptides facilitate targeted delivery of CF to the placenta. (**A**) Size distribution (in nanometer) of peptide-decorated liposomes. (**B** to **J**) Peptide-decorated liposomes (red) containing CF (green) were injected (100 μl per mouse) into the tail vein of pregnant mice at E12.5. After 24 hours, mice were subjected to cardiac perfusion to remove unbound liposomes. Placentas were collected, fixed, and frozen; evidence of liposome binding was assessed by confocal microscopy. $n = 3$ placentas from $n = 3$ mice were examined. Representative confocal images are shown. (B to D) TAMRA-CGKRK. (E to G) Rhodamine-iRGD. (H to J) TAMRA-ARA. Red, peptide; green, CF cargo; blue, DAPI (nuclei). Scale bars, 50 μm. (**K** to **M**) Term placental explants were incubated with peptide-decorated liposomes (100 μl) for 24 hours. Binding and uptake were assessed by fluorescence microscopy ($n = 3$). (K) TAMRA-CGKRK ($n = 3$). (L) Rhodamine-iRGD ($n = 3$). (M) TAMRA-ARA ($n = 3$). Red, peptide; green, CF cargo; blue, DAPI (nuclei). Scale bars, 50 μm. AU, arbitrary units.

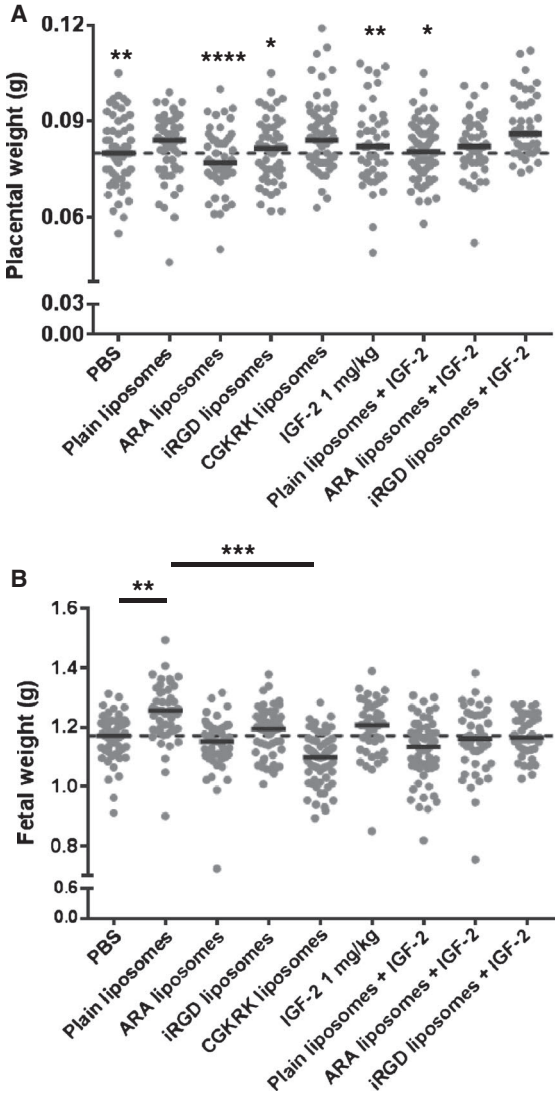

Fig. 7. Targeted delivery of IGF-2 increases placental weight in wild-type C57BL/6J mice. Pregnant mice (N = dams, n = fetuses) were intravenously injected with 100 µl of PBS (N = 8, n = 59), plain (undecorated) liposomes (N = 8, n = 49), empty ARA–decorated liposomes (N = 8, n = 53), iRGD-decorated liposomes (N = 8, n = 56), CGKRK-decorated liposomes (N = 9, n = 62), free IGF-2 (1 mg/kg maternal body weight; N = 8, n = 43), plain liposomes (N = 9, n = 68), ARA liposomes (N = 8, n = 45), or iRGD liposomes (N = 8, n = 43) containing IGF-2 (approximately 0.3 mg/kg maternal body weight) on E11.5, E13.5, E15.5, and E17.5. (**A** and **B**) Mice were sacrificed at E18.5; fetal (A) and placental (B) weights were measured. Data points represent individual conceptuses; horizontal line represents median. (A) *P < 0.05, **P < 0.01, ***P < 0.001, ****P < 0.0001 compared to animals treated with iRGD liposomes containing IGF-2; (B) **P < 0.01, ***P < 0.001 compared to animals treated with plain liposomes; Kruskal-Wallis test with Dunn's multiple comparison post hoc test.

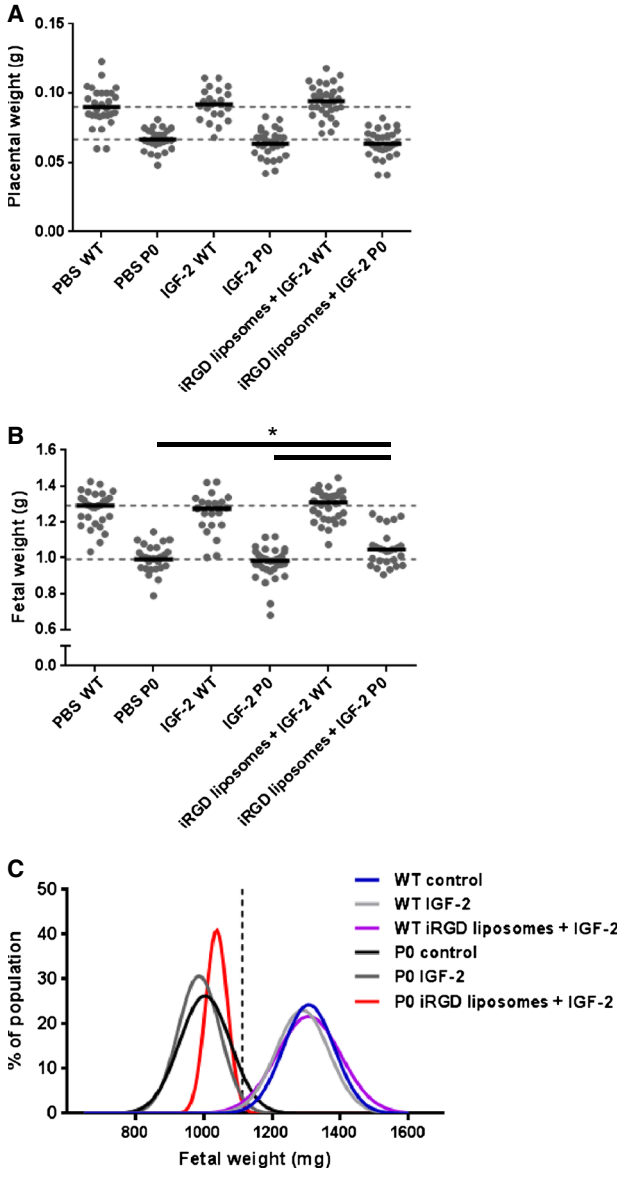

Fig. 8. Targeted delivery of IGF-2 improves fetal weight distribution in the P0 mouse model of FGR. Pregnant mice (N = dams, n = fetuses) were injected on E11.5, E13.5, E15.5, and E17.5 with 100 µl of free IGF-2 (1 mg/kg maternal body weight; N = 8, n = 53) or iRGD-decorated liposomes containing IGF-2 (approximately 0.3 mg/kg maternal body weight; N = 8, n = 60), or were untreated/PBS-injected controls (N = 8, n = 56). (**A** to **C**) Mice were sacrificed at E18.5; placental (A) and fetal (B) weights were measured, and a fetal weight population distribution curve was plotted (C). Data points in (A) and (B) represent individual conceptuses; horizontal lines represents mean (A) or median (B); horizontal dashed lines represent mean/median value of the wild-type (WT) and P0 controls. Vertical dashed line in (C) represents the fifth weight centile (in milligram) of control WT mice. P0 fetal weights were significantly increased in mice treated with iRGD-decorated IGF-2 liposomes compared to controls or mice treated with free IGF-2 (P < 0.05); weight variation was significantly reduced (P < 0.05, F test of equality of variances). Data obtained from PBS-injected mice (n = 3) were combined with those from untreated animals (n = 5) because mean fetal and placental weights were not significantly different.

human placenta (*36*); however, our data identify calreticulin as a putative receptor on the placental surface. We did not identify p32 in our mouse placental chromatography eluents, by either mass spectrometry or immunoblotting, and we could not detect p32 expression on the surface of human placental MVM vesicles (fig. S7E). Calreticulin, originally identified as a calcium-binding protein in the endoplasmic reticulum that regulates intracellular calcium homeostasis (*37*), also acts as a molecular chaperone (*38*), modulates cell adhesion (*39*), and promotes anticancer immune responses (*40*, *41*). Calreticulin binds the synthetic peptide KLGFFKR (*42*), which, like CGKRK, has basic amino acid residues at the C terminus. Increased calreticulin expression enhances proliferation, migration, and extracellular matrix degradation in cancer cells (*43*), behaviors that are common to some human and mouse trophoblast lineages. Because total calreticulin protein expression is reportedly increased in preeclamptic placentas (*44*), CGKRK-mediated targeting may represent a novel means of delivering therapeutics to the poorly functioning placenta; however, the decrease in fetal weight observed following treatment with empty CGKRK–decorated liposomes will require further investigation.

The biological consequences of administering homing peptides to healthy organs and tissues have not previously been assessed; this proof-of-concept study did not detect any detrimental effect of targeting peptides on pregnancy outcome in mice, and no evidence of fetal transfer of targeted peptides or targeted liposomes was observed. Furthermore, IGF-2 encapsulated in iRGD-decorated liposomes did not increase the weight of the maternal kidney or spleen, providing evidence of the transient passage of these targeted nanoparticles through the clearance organs. In human tissue, extended culture of targeting peptides with placental explants had no detrimental effect on trophoblast proliferation or apoptosis, suggesting that they do not interfere with normal placental function at the dose tested.

Technologies that can target therapeutics directly to their site of action, minimizing interactions with other tissues, will circumvent the risks and side effects potentially associated with systemic administration of drugs in human pregnancy and should expedite translation of new treatments into the clinic. To achieve this, further research and development will be required, including optimization of liposomal formulation, drug encapsulation protocols, and dosing regimens to maximize drug delivery, combined with toxicity testing in appropriate animal models. Beyond this, we foresee a scenario where the safety and specificity of targeting could be tested by administering empty liposomes before pregnancy termination, followed by evaluation of drug-loaded liposomes in a cohort of women with severe FGR and a high risk of poor pregnancy outcome. Although we recognize that our technology may have detrimental off-target effects in women with undiagnosed malignancies, we believe that the benefits would greatly outweigh the possible risks, and a screening program before treatment could be implemented. In summary, our technology, for which we provide proof-of-principle results using IGF-2–containing liposomes targeted with iRGD, will provide a platform to develop the first generation of placenta-specific therapeutics, which will represent the first treatment options for serious pregnancy complications whose causes are rooted in suboptimal placental function, such as PE and FGR.

MATERIALS AND METHODS

Study design

The objective of this study was to create a biocompatible nanoparticle for targeted delivery of therapeutics to the placenta. Previously described tumor-homing sequences were screened for their ability to selectively accumulate in the mouse placenta in vivo; quantitation of placental enrichment was assessed by phage display. Peptide-decorated nanoworms and liposomes were synthesized, and their ability to selectively target the mouse placenta was assessed by fluorescence microscopy. These in vivo screening experiments were undertaken using three to four mice per group, and a minimum of three randomly selected placentas from each mouse were examined. For preclinical studies, each experimental group included 8 to 10 mice per group, based on previous studies undertaken in the Maternal and Fetal Health Research Centre, and was sufficient to determine statistically significant differences in fetal and placental weights. Animals were randomly assigned to experimental groups, studies were not blinded, and the endpoint was term pregnancy (E18.5). Fetal/placental weights from resorbing conceptuses were the only data excluded from the study. Ex vivo binding of peptides and liposomes to human placental explants and immunostaining of mouse placental tissue were assessed by examining a minimum of three randomly selected tissue sections from each of the three randomly sampled tissue explants or randomly selected mouse placentas obtained from three to four individual human placentas/animals per group. The receptor for CGKRK was captured using affinity chromatography and identified using MALDI-TOF mass spectrometry. In vitro studies of calreticulin-CGKRK interactions were performed a minimum of $n = 3$ times.

Animal procedures

BALB/c mice (Charles River), C57BL/6J mice, and placenta-specific P0 knockout mice (P0 mice) with deletion of the U2 exon within the *Igf2* gene were housed, and all procedures were performed according to procedures approved by the Animal Research Committees at University of California, Santa Barbara, or in accordance with the UK Animals (Scientific Procedures) Act 1986 at the University of Manchester. Animals had free access to food and water and were maintained on a 12-hour light/12-hour dark cycle at 21° to 23°C. Following mating, the presence of a copulation plug was denoted as embryonic day 0.5 (E0.5) of pregnancy. P0 mice were originally a gift from M. Constância (Babraham Institute, UK). Heterozygous males with the P0 deletion were mated with C57BL/6J female mice (wild type; 6 to 10 weeks of age, which resulted in mixed litters consisting of both wild-type and P0 fetuses) (*25*).

Phage homing

The T7-select phage display system (EMD Biosciences) was used to construct peptide phage libraries. Individual phages were cloned according to the manufacturer's instructions, as previously described (*45*, *46*). Amplified phages were purified from bacterial lysate by precipitation with PEG-8000 (Sigma-Aldrich), cesium chloride gradient ultracentrifugation, and dialysis. The identity of the displayed peptides was confirmed by sequencing of the insert-containing region at the C terminus of the T7 major coat protein gp10 (Eton Bioscience). To test homing of individual phage clones in vivo, 1×10^{10} phage in PBS were intravenously injected via the tail vein. Terminal cardiac perfusion was performed after 30 min to remove unbound phage; major organs were harvested, weighed, and homogenized in LB bacterial growth medium containing 1% (v/v) NP-40. Phage titers (wet tissue mass^{-1}) were determined, and the data were expressed as fold enrichment in comparison to the titer of the control phage G7 (displaying the surface peptide GGGGGGG) in the same tissue (*45*, *46*).

Peptide synthesis

Peptides were synthesized in-house at the University of California, Santa Barbara, using Fmoc chemistry in a solid-phase synthesizer and purified by high-performance liquid chromatography, and their sequence and structures were confirmed by mass spectrometry as previously described (*45*) or were purchased from Insight Biotechnology.

Peptide targeting

Individual synthetic peptides (200 μg) labeled with FAM were administered via tail vein injection to pregnant BALB/c mice (E11.5 to E17.5) and allowed to circulate for 3 hours. Following terminal cardiac perfusion with PBS to remove unbound peptide, tissues were collected for analysis. Organs were snap-frozen or fixed in paraformaldehyde [4% (w/v) in PBS; overnight], cryoprotected in sucrose solution [30% (w/v) in PBS; 24 hours], embedded in optimal cutting temperature (OCT; Sakura), and stored at −80°C. Tissue sections (8 μm) were fixed in ice-cold methanol (15 min), washed in PBS (2×; 5 min), mounted in Vectashield mounting medium containing DAPI (Vector Laboratories), and examined on an Olympus Fluoview 500 confocal microscope (Olympus America). Images were captured at the same exposure so that comparisons across samples could be made.

Peptide treatment study

BALB/c mice were intravenously injected with vehicle (PBS), Ac-iRGD, or Ac-CGKRK (100 μg) on E11.5, E13.5, and E15.5 of pregnancy. Mice were sacrificed at E18.5, and the following parameters were measured: litter size, resorption number, fetal weight, placental weight, fetal/placental weight ratio, and percent increase in maternal body weight from E10.5 to E18.5. The number of animals required to observe a statistically significant change in fetal and/or placental weight following treatment (n = 8 to 10 mice per group) was determined by a power calculation performed using data from previous treament studies. Placentas were fixed in paraformaldehyde [4% (w/v) in PBS; overnight], dehydrated in sucrose solution [30% (w/v) in PBS; 24 hours], then embedded in OCT, and stored at −80°C.

Peptide-conjugated nanoworms

Peptide-conjugated iron oxide nanoworms were prepared as previously described (*23*, *24*, *47*). Nanoworms (5 mg of iron/kg maternal body weight) were intravenously injected into pregnant BALB/c mice (E12.5 to E15.5; n = 3 per nanoworm formulation) and allowed to circulate for 5 hours. After cardiac perfusion with PBS to remove unbound nanoworms, organs were harvested, snap-frozen, and stored at −80°C. Tissue sections (8 μm) were fixed in ice-cold methanol (15 min), washed in PBS (2×; 5 min), mounted in Vectashield mounting medium containing DAPI, and examined on an Olympus Fluoview 500 confocal microscope. Images were captured at the same exposure so that comparisons across samples could be made.

Liposome preparation

Liposomes were prepared using the thin lipid film process. The constituent lipids were as follows: 1,2-distearoyl-*sn*-glycero-3-phosphocholine (DSPC; 32.5 mM), 1,2-distearoyl-*sn*-glycero-3-phosphoethanolamine-*N*-[methoxy(polyethylene glycol)-2000] ammonium salt [DSPE-PEG(200); 1.875 mM], 1,2-distearoyl-*sn*-glycero-3-phosphoethanolamine-*N*-[maleimide(polyethylene glycol)-2000] ammonium salt [DSPE-PEG(2000)-maleimide; 0.625 mM; Avanti Polar Lipids], and cholesterol (15 mM; Sigma-Aldrich). These were dissolved in approximately 10 ml of chloroform (Sigma-Aldrich) in a round-bottom flask. The chloroform was removed by rotary evaporation (40°C, 270 mbar) to form a lipid film and incubated in a vacuum oven drier overnight at room temperature. The film was rehydrated in 1 ml of PBS containing FAM [CF, 2.5 mM; Sigma-Aldrich; reconstituted first in 0.1% (v/v) dimethyl sulfoxide] or IGF-2 (40 μM; GroPep; maximal dose of 1 mg/kg in 100 μl of liposomes, if 100% encapsulation was attained; IGF-2 was reconstituted first in 10 mM HCl), and the resulting suspension was vortexed (10 to 15 min), heated at 45°C for a minimum of 2 hours, and extruded through a 1-ml-size thermobarrel Mini-Extruder (100-nm-pore polycarbonate membranes; Avanti Polar Lipids) a minimum of 11 times to produce a monodisperse liposome preparation containing encapsulated CF or IGF-2.

To prepare targeted liposomes, peptides bearing an N-terminal cysteine moiety [TAMRA-CGGGCGKRK (CGKRK); rhodamine-CCRGDKGPDC (iRGD); 1.25 μM; Insight Biotechnology] were incubated with extruded liposomes for a minimum of 4 hours at room temperature to facilitate conjugation of free thiol groups on the cysteine residues to maleimide groups on the liposomal surface via a Michael-type addition reaction. The nontargeting peptide sequence TAMRA-ARA was conjugated to the liposome surface in a similar manner to produce control liposomes. Because of the cyclic structure of iRGD, rhodamine was used instead of TAMRA for ease of synthesis; both fluorophores have similar molecular weights (rhodamine, 479 daltons; TAMRA, 527.5 daltons), and this substitution did not affect the selectivity of peptide targeting.

To remove unbound peptide or unencapsulated CF, liposomes were dialyzed against PBS (8×, 500 ml; 24 hours) in Slide-A-Lyzer dialysis cassettes with a molecular weight cutoff (MWCO) of 3.5 kD (Thermo Fisher Scientific). To remove unencapsulated IGF-2 from the preparations, liposomes were dialyzed in cassettes with a 10-kD MWCO. The liposomes were stored at 4°C; Z-average sizes were calculated from the size distributions measured by dynamic light scattering at 25°C (Zetasizer Nano ZS).

Liposome targeting

Control or targeted liposomes (100 μl) were administered via tail vein injection to pregnant C57BL/6J mice at E12.5 and allowed to circulate for 24, 48, or 72 hours (n = 3 per group). Following terminal cardiac perfusion with PBS, tissues were collected for analysis. Organs were fixed in paraformaldehyde [4% (w/v) in PBS; overnight], embedded in OCT (Sakura), and stored at −80°C. Tissue sections (10 μm) were fixed in paraformaldehyde [4% (w/v) in PBS; 15 min], washed in PBS (2×; 5 min), mounted in Vectashield mounting medium containing DAPI (Vector Laboratories), and examined on a Zeiss Axio Observer fluorescence microscope. Images were captured at the same exposure so that comparisons across samples could be made.

Liposome treatment study

Pregnant C57BL/6J mice were intravenously injected with 100 μl of vehicle (PBS); plain (undecorated) liposomes; empty ARA–, iRGD-, or KRK-decorated liposomes; free IGF-2 (1 mg/kg maternal body weight) or plain liposomes; ARA liposomes; or iRGD liposomes containing IGF-2 (approximately 0.3 mg/kg maternal body weight) on E11.5, E13.5, E15.5, and E17.5 of pregnancy. Pregnant P0 mice followed the same dosing regime and were intravenously injected with 100 μl of vehicle (PBS), free IGF-2 (1 mg/kg maternal body weight), or iRGD liposomes containing IGF-2 (approximately 0.3 mg/kg maternal body weight). All mice were sacrificed at E18.5, and the following variables

were measured: fetal weight, placental weight, litter size, number of resorptions, maternal spleen weight, and maternal kidney weight.

The number of animals required to observe a statistically significant change in fetal and/or placental weight following treatment (n = 8 to 10 mice per group) was determined by a power calculation performed using data from previous treament studies. Organs were fixed in paraformaldehyde [4% (w/v) in PBS; overnight], dehydrated in sucrose solution [30% (w/v) in PBS; 24 hours], then embedded in OCT, and stored at −80°C.

Human tissue

First-trimester placentas were collected following surgical or medical termination of pregnancy. Term placentas (37 to 42 weeks of gestation) were obtained from uncomplicated pregnancies within 30 min of vaginal or cesarean delivery. Written informed consent was obtained from all patients, and the study was performed in accordance with the North West Local Research Ethics Committee approvals 08/H1010/28 and 08/H1010/55. Villous tissue was randomly sampled, and biopsies were washed in serum-free culture medium and dissected into 3-mm^3 explants under sterile conditions. Explants (one per well) were submerged in 1 ml of culture medium [1:1 ratio of Dulbecco's modified Eagle's medium (DMEM) and Ham's F12 medium (Lonza Biosciences) containing glutamine (2 mM), penicillin (100 IU/ml), streptomycin (100 μg/ml), and 10% (v/v) fetal bovine serum (Invitrogen)] in 24-well culture plates precoated with agarose [1% (w/v); Sigma-Aldrich]. Explants were maintained in 20% O_2, 5% CO_2 at 37°C for up to 72 hours, as previously described (*26*, *48*).

Explant culture

First-trimester placental explants were serum-starved overnight and then cultured with vehicle (PBS), Ac-CGKRK, or Ac-iRGD (20 μM; 24 to 48 hours; n = 4 independent experiments). After washing in PBS, tissue was fixed in neutral buffered formalin [4% (v/v), pH 7.4; overnight], dehydrated, and paraffin-embedded.

Peptide-binding assay

Term villous placental explants (3 mm^3) were added to individual Eppendorf containing prewarmed culture medium [DMEM/Ham's F12 medium containing glutamine (2 mM), penicillin (100 IU/ml), streptomycin (100 μg/ml), and 10% (v/v) fetal bovine serum] and either FAM-CGKRK (20 μM), FAM-iRGD (20 μM), or vehicle control (PBS). Explants were incubated at 37°C in the dark for up to 3 hours, washed in PBS (1×; 5 min), fixed in neutral buffered formalin [4% (v/v), pH 7.4; overnight], and embedded in OCT. Pulse-chase experiments were also performed: Explants were incubated with FAM-labeled peptide (20 μM) for 3 hours, washed in PBS (1×; 5 min), placed in fresh culture medium, and incubated for a further 21 hours before fixation. Tissue sections (8 μm) were fixed in ice-cold methanol (15 min), washed in PBS (2×; 5 min), mounted in Vectashield mounting medium containing DAPI (Vector), and examined on a Zeiss Axio Observer fluorescence microscope. Images were captured at the same exposure so that comparisons across samples could be made. n = 4 independent experiments were performed.

Liposome-binding assay

Term placental explants were placed in 24-well plates precoated with agarose [1% (w/v) in DMEM/Ham's F12 medium containing glutamine (2 mM), penicillin (100 IU/ml), streptomycin (100 μg/ml), and 10% (v/v) fetal bovine serum]. Explants were incubated with either control or targeted liposomes containing CF (100 μl per well) for 24 hours at 37°C in the dark. Tissue was washed in PBS (1×; 5min), fixed in neutral buffered formalin [4% (v/v), pH 7.4; overnight], and embedded in OCT. Sections were cut, processed, and visualized as described above. n = 3 independent experiments were performed.

Calreticulin knockdown

siRNA sequences added to the culture medium of human term placental explants in the absence of transfection reagents or electroporation spontaneously accumulate in the STB layer (*48*). Calreticulin knockdown was achieved by adding siRNA sequences directly to the culture medium (50 nM; sequence 1, #HSS101319; sequence 2, #HSS188554; Stealth Select RNAi siRNA, Invitrogen). A nontargeting siRNA was used as a negative control (#12935300; Invitrogen). Term placental explants were cultured with vehicle (PBS), nontargeting siRNA, or the calreticulin-specific siRNA sequences for 72 hours. Efficiency of knockdown was determined by quantitative real-time polymerase chain reaction (qRT-PCR) and immunohistochemistry. n = 4 independent experiments were performed.

Quantitative RT-PCR

Total RNA was extracted from placental explants, quantified, and reverse-transcribed (100 ng per sample) as previously described using an AffinityScript Multiple Temperature cDNA Synthesis Kit (Agilent) (*49*). Calreticulin complementary DNA (cDNA) was amplified using qPCR using published primer sequences (forward, 5′-TGGCGTGCTGGGCCTGGACCTCTGG-3′; reverse, 5′-CCTCTTTGCGTTTCTTGTCTTCTTC-3′; Invitrogen) (*50*) and Ultra-Fast SYBR Green QPCR Master Mix with 5-carboxy-X-rhodamine as a passive reference dye (Agilent) in a Stratagene Mx3000P RT-PCR machine. Calreticulin mRNA expression in triplicate samples was quantified against a standard curve constructed with cDNA obtained from human reference total RNA (Agilent). Calreticulin expression was normalized to the expression of the housekeeping gene *18S rRNA* (forward primer, 5′-GCTGGAATTACCGCGGCT-3′; reverse primer, 5′-CGGCTACCACATCCAAGGAA-3′).

Saturation-binding assay

Binding of CGKRK to recombinant human calreticulin was quantified as previously described (*35*). Microplate wells precoated with calreticulin protein (3 μg/ml; Stratech) were incubated with increasing concentrations of FAM-CGKRK in PBS (100 μl per well) for 1 hour at room temperature. After washing with ice-cold PBS containing 0.01% (v/v) Tween 20 and 0.2 M NaCl (5×; 5 min), fluorescence (excitation, 485 nm; emission, 538 nm) was measured using a SpectraMax Gemini XS microplate reader (Molecular Devices). Values were normalized to nonspecific peptide binding, measured in the absence of calreticulin. n = 4 independent experiments were performed.

Quantification of peptide binding following calreticulin knockdown

Following calreticulin knockdown, explants were transferred from culture plates into individual Eppendorf containing prewarmed culture medium. Explants were incubated with FAM-CGKRK (20 μM) or vehicle control (PBS) at 37°C in the dark for 30 min, during which time peptide binding occurred. Explants were washed in PBS (2×; 5 min) and transferred to fresh tubes containing 1 ml of distilled water (dH_2O). Explants were frozen (−80°C, 30 min) and thawed (37°C, 5 min) to

promote tissue lysis and peptide release from the syncytium. Tubes were briefly vortexed, and the explants were removed and blotted to remove excess liquid. The explants were weighed, and the tubes were centrifuged (13,250*g*, 10 min) to pellet residual cell debris. Supernatants were transferred in triplicate (3×, 200 µl) to a 96-well plate, fluorescence (excitation, 485 nm; emission, 538 nm) was quantified using a SpectraMax Gemini XS microplate reader, and values were normalized to the wet weight of the explant. $n = 4$ independent experiments were performed.

Isolation of STB microvillus membrane vesicles

MVM vesicles were prepared from normal human term placenta by Mg^{2+} precipitation and differential centrifugation, as previously described (*51*). MVM vesicles spontaneously orientate right-side-out, replicating the extracellular surface of the placenta. Briefly, placental tissue (350 g) was homogenized with 2.5 volume of ice-cold mannitol buffer [300 mM mannitol, 1 mM $MgSO_4$, 10 mM Hepes-tris (pH 7.4)]. Following the addition of $MgCl_2$ (10 mM), the homogenate was stirred (10 min on ice) before centrifugation (2300*g*, 15 min). The supernatant was collected and centrifuged (23,500*g*, 40 min; Sorvall Discovery 100SE), the pellet was resuspended in 2.5 ml of mannitol buffer and then stirred with $MgCl_2$ (10 mM; 10 min on ice), and the two centrifugation steps were repeated again. The final pellet was weighed and resuspended in 6 ml of intravesicular buffer [20 mM sucrose, 5 mM Hepes, 5 mM tris (pH 7.4)], and membranes were vesiculated by passing 20 times through a 25-gauge needle. MVM protein concentration was determined by the Lowry method, and MVM purity was assessed by measuring enrichment of alkaline phosphatase activity, as previously described (*51*). Vesicles were stored at 4°C and used within 48 hours of isolation.

Flow cytometry

To quantify calreticulin expression in the MVM, MVM vesicles suspended in 1 ml of PBS (2 mg of protein/ml) were incubated with a rabbit anti-human calreticulin primary antibody (1:100; Abcam), a rabbit anti-human p32 primary antibody (1:200; Sigma-Aldrich), or a rabbit IgG control (Sigma-Aldrich) for 1 hour at room temperature on a rotating wheel. PBS was added in excess, and MVM vesicles were incubated for a further 15 min. After centrifugation (23,500*g*, 40 min; Sorvall Discovery 100SE), the supernatant was removed, and the vesicles were resuspended in PBS containing a fluorescein isothiocyanate–conjugated secondary antibody (1:50; Dako). MVM vesicles were incubated for 30 min at room temperature on a rotating wheel, PBS was added in excess, and vesicles were incubated for a further 15 min. MVM vesicles were pelleted by centrifugation (23,500*g*, 40 min) and resuspended in PBS, and the extent of antibody binding was quantified using a Beckman Coulter CyAn ADP flow cytometer with Summit analysis software. MVM vesicles from $n = 4$ placentas were analyzed.

To quantify FAM-CGKRK binding to the MVM, MVM vesicles suspended in PBS (2 mg of protein; 1-ml final volume) were incubated with either a control protein (BSA; 10 µg) or recombinant human calreticulin (10 µg; Stratech) and FAM-CGKRK (20 µM) for 30 min at room temperature on a rotating wheel. PBS was added in excess, and vesicles were incubated for a further 15 min. Vesicles were centrifuged (23,500*g*, 40 min) and resuspended in PBS, and the extent of peptide binding was quantified using a CyAn ADP flow cytometer. MVM vesicles from $n = 4$ placentas were analyzed.

Affinity chromatography and mass spectrometry

To identify putative homing peptide receptors, affinity chromatography and mass spectrometry were performed as previously described (*46*). Briefly, mouse placental tissue (E16.5; one placenta from each of three mice) was snap-frozen and crushed to a powder with a pestle and mortar. Tissue (100 mg/400 µl) was incubated in tissue lysis buffer [ice-cold PBS containing *n*-octyl-β-D-glucopyranoside (200 nM; Calbiochem) and four EDTA-free protease inhibitors cocktail tablets (Roche)] on a shaker at 4°C for 6 hours. The homogenate was centrifuged (22,000*g*, 30 min; 4°C), and the supernatant was retained. CGKRK peptide was coupled to two SulfoLink resin columns (Pierce) according to the manufacturer's instructions, which were equilibrated with column wash buffer (ice-cold PBS containing 50 nM n-octyl-β-D-glucopyranoside; 3×, 1-ml washes). Tissue supernatant (1 ml) was added to the columns and incubated overnight at 4°C on a rotating shaker. The supernatant was discarded, and the columns were washed (8×, 4 ml) with column wash buffer. Bound peptides were eluted from one column by serial application of free CGKRK peptide in wash buffer (2 mM peptide; 10×, 0.4-ml elutions). A control peptide (CREKA; 2 mM) was applied to the second column to detect nonspecific protein binding. Eluted fractions were collected, analyzed for protein expression, and separated using SDS–polyacrylamide gel electrophoresis (SDS-PAGE). Bands were visualized using a SilverSnap SDS-PAGE silver staining kit (Pierce); bands appearing in elutions from the CGKRK column, but not from the control peptide column, were excised. Proteins were digested with trypsin, and the resulting peptides were analyzed using MALDI-TOF mass spectrometry. Profound software was used to match peptide data against known protein sequences.

Immunofluorescence

Tissue sections (8 µm) were fixed in ice-cold methanol (15 min), washed in PBS (2×; 5 min), and incubated with 5% (w/v) BSA in PBS for 30 min to block nonspecific binding sites. Primary antibodies [rabbit anti-cytokeratin, wide spectrum screening (1:50; Z0622, Dako); rat anti-mouse pan endothelial cell antigen MECA-32 (1:50; sc-19603, Santa Cruz Biotechnology); rabbit anti-human calreticulin (1:100; ab2907, Abcam); rabbit anti-mouse α_V integrin (1:100; AB1930, Millipore); rabbit anti-mouse Ki67 (1:200; ab16667, Abcam); rabbit anti-mouse cleaved caspase-3 (1:50; #9661, Cell Signaling); rabbit anti-mouse cathepsin Q (1:250; ab171840, Abcam); rabbit anti-mouse GCM-1 (1:250; sc-98811, Santa Cruz Biotechnology); rabbit anti-mouse Tpbpa (1:500; ab104401, Abcam); isotype control mouse or rabbit IgG (concentration matched; I8765 and I8140, Sigma-Aldrich); and control rat IgG (concentration matched; sc-2026, Santa Cruz Biotechnology)] were diluted in PBS and applied to the tissue sections. Slides were incubated for 1 hour at room temperature in a humidity chamber. After washing in PBS (3×, 5 min), tissue sections were incubated with the appropriate secondary antibodies [anti-mouse, A11004; anti-rabbit, A1101; or anti-rat, A11077 Alexa Fluor 568 (1:500); Invitrogen] for 1 hour at room temperature. After further PBS washes, slides were mounted in Vectashield mounting medium containing DAPI (Vector) and examined using a Zeiss Axio Observer fluorescence microscope. For each antibody, images were captured at the same exposure so that comparisons between samples could be made.

To quantify Ki67 and cleaved caspase-3 immunostaining, three random images of the placental labyrinth and the decidua were captured, and the number of immunopositive cells per field was counted by a blinded observer. These data were used to determine a mean number of positive cells within the labyrinth and decidua of each placenta. $n = 3$ placentas from $n = 4$ mice per treatment group were examined.

Immunohistochemistry

Sections of wax-embedded placental explants (5 μm) were deparaffinized in Histo-Clear and alcohol, washed in dH_2O, and microwaved for 10 min in sodium citrate buffer [0.01 M; containing 0.05% (v/v) Tween 20 (pH 6.0)] to facilitate antigen unmasking. After cooling, endogenous peroxide activity was blocked by incubating the tissue sections in 3% (v/v) hydrogen peroxide for 10 min. Tissue sections were washed three times in 0.05 M tris-buffered saline (TBS) and incubated with 5% (w/v) BSA in TBS for 30 min to block nonspecific binding. Primary antibodies [diluted to the required concentration with 0.05 M TBS (pH 7.6); mouse anti-human Ki67 (1:200; clone MIB-1, #M7240, Dako), mouse anti-human M30 CytoDEATH (1:50; #12-140-322-001, Roche), rabbit anti-human calreticulin (1:100; ab2907, Abcam), and isotype control mouse or rabbit IgG (concentration matched; I8765 and I8140, Sigma-Aldrich)] were applied to the tissue sections, which were incubated overnight at 4°C in a humidity chamber. Slides were washed (3×, 5 min; TBS), and the secondary antibodies, diluted in TBS (biotinylated goat anti-mouse IgG, 1:200; Dako), were applied for 30 min at room temperature. Slides were washed again (3×, 5 min; TBS) and incubated with avidin peroxidase (5 μg/ml in TBS; Sigma-Aldrich) for 30 min at room temperature. Slides were washed in TBS and incubated for 1 to 5 min with 0.05% (w/v) diaminobenzidine and 0.015% (v/v) hydrogen peroxide (Sigma-Aldrich). Slides were washed in dH_2O, counterstained with hematoxylin, dehydrated in alcohol and Histo-Clear, and mounted in DPX (Sigma-Aldrich).

To quantify human CTB proliferation and apoptosis after immunostaining for Ki67 and M30, six random images of each immunostained explant were captured. The number of Ki67- or M30-positive CTB was counted by a blinded observer and expressed as a percentage of the total number of CTB in the field of view; these data were used to determine a mean number of positive CTB for each explant. $n = 4$ independent experiments were performed.

Genotyping of P0 fetuses

DNA was extracted from fetal tail tips using a DNeasy extraction kit (Qiagen). *Igf2* $P0^{+/-}$ mutants were identified using a primer pair to amplify a 740–base pair (bp) fragment across the 5-kb deletion (sense, 5′-TCCTGTACCTCCTAACTACCAC-3′; antisense, 5′-GAGCCAGAAGCAAACT-3′) with a third primer amplifying a 495-bp fragment from the wild-type allele (5′-CAATCTGCTCCTGCCTG-3′), as previously described (*52*).

IGF-2 ELISA

To quantify the amount of IGF-2 encapsulated, liposomes (100 μl) were lysed (Triton X-100; 0.5% in dH_2O; 200 μl; 20 min, 37°C), sonicated (30 min; Ultrawave Ltd.), and centrifuged (1 hour, 13,000 rpm; Heraeus Pico 21, Thermo Scientific). The supernatant and the pellet were assayed separately by ELISA (human IGF-2 ELISA; MEDiagnostics) according to the manufacturer's instructions. The concentration of IGF-2 in the supernatant and the pellet were added together to calculate the total concentration of drug (free within the lipid core and bound to the lipid wall) administered in each liposome bolus.

Data analysis

Data were analyzed using GraphPad Prism software (version 5). Nonparametric data were expressed as medians and analyzed using Kruskal-Wallis test, and parametric data were expressed as means and analyzed using analysis of variance (ANOVA) or Student's *t* test. Frequency distribution curves were created by constructing fetal weight histograms and performing nonlinear regression (Gaussian distribution), as previously described (*53*). Data from a minimum of three independent experiments are presented. Significance was taken as $P < 0.05$, unless otherwise stated.

SUPPLEMENTARY MATERIALS

Supplementary material for this article is available at http://advances.sciencemag.org/cgi/content/full/2/5/e1600349/DC1

fig. S1. The tumor-homing peptides FAM-CGKRK and FAM-iRGD do not accumulate in maternal organs of pregnant mice.
fig. S2. FAM-CGKRK and FAM-iRGD colocalize with endothelial cell and trophoblast markers in the mouse placenta.
fig. S3. FAM-CGKRK and FAM-iRGD colocalize with markers of the mouse placental labyrinth.
fig. S4. Administration of placental homing peptides does not alter cell turnover in the developing mouse placenta.
fig. S5. FAM-CGKRK and FAM-iRGD colocalize with markers villous trophoblast.
fig. S6. FAM-iRGD colocalizes with α_v integrin in mouse decidual spiral arteries.
fig. S7. Calreticulin knockdown in the STB layer of human term placental explants.
fig. S8. Biodistribution of tumor-homing peptide–decorated nanoworms in pregnant mice.
fig. S9. Biodistribution of tumor-homing peptide–decorated liposomes in pregnant mice after 24 hours.
fig. S10. Biodistribution of tumor-homing peptide–decorated liposomes in pregnant mice after 72 hours.
fig. S11. Biodistribution of liposomes decorated with a control peptide in pregnant mice.
fig. S12. Biodistribution of plain liposomes (no targeting peptide) in pregnant mice.
fig. S13. Targeted delivery of IGF-2 to wild-type C57BL/6J mice does not alter litter size, resorption number, or weight of maternal clearance organs.
fig. S14. Targeted delivery of IGF-2 to P0 mice does not alter litter size, resorption number, or weight of maternal clearance organs.

REFERENCES AND NOTES

1. A. P. MacKay, C. J. Berg, H. K. Atrash, Pregnancy-related mortality from preeclampsia and eclampsia. *Obstet. Gynecol.* **97**, 533–538 (2001).
2. J. Uzan, M. Carbonnel, O. Piconne, R. Asmar, J.-M. Ayoubi, Pre-eclampsia: Pathophysiology, diagnosis, and management. *Vasc. Health Risk Manag.* **7**, 467–474 (2011).
3. M. L. Chiswick, Intrauterine growth retardation. *Br. Med. J.* **291**, 845–848 (1985).
4. C. P. Sibley, M. A. Turner, I. Cetin, P. Ayuk, C. A. R. Boyd, S. W. D'Souza, J. D. Glazier, S. L. Greenwood, T. Jansson, T. Powell, Placental phenotypes of intrauterine growth. *Pediatr. Res.* **58**, 827–832 (2005).
5. J. C. P. Kingdom, S. J. Burrell, P. Kaufmann, Pathology and clinical implications of abnormal umbilical artery Doppler waveforms. *Ultrasound Obstet. Gynecol.* **9**, 271–286 (1997).
6. P. D. Gluckman, M. A. Hanson, C. Cooper, K. L. Thornburg, Effect of in utero and early-life conditions on adult health and disease. *N. Engl. J. Med.* **359**, 61–73 (2008).
7. L. Doridot, B. Passet, C. Méhats, V. Rigourd, S. Barbaux, A. Ducat, F. Mondon, M. Vilotte, J. Castille, M. Breuiller-Fouché, N. Daniel, F. le Provost, A.-L. Bauchet, V. Baudrie, A. Hertig, C. Buffat, U. Simeoni, G. Germain, J.-L. Vilotte, D. Vaiman, Preeclampsia-like symptoms induced in mice by fetoplacental expression of STOX1 are reversed by aspirin treatment. *Hypertension* **61**, 662–668 (2013).
8. J. L. Stanley, I. J. Andersson, C. J. Hirt, L. Moore, M. R. Dilworth, A. R. Chade, C. P. Sibley, S. T. Davidge, P. N. Baker, Effect of the anti-oxidant tempol on fetal growth in a mouse model of fetal growth restriction. *Biol. Reprod.* **87**, 1–8 (2012).
9. J. L. Stanley, I. J. Andersson, R. Poudel, C. F. Rueda-Clausen, C. P. Sibley, S. T. Davidge, P. N. Baker, Sildenafil citrate rescues fetal growth in the catechol-*O*-methyl transferase knockout mouse model. *Hypertension* **59**, 1021–1028 (2012).
10. N. M. Fisk, R. Atun, Market failure and the poverty of new drugs in maternal health. *PLOS Med.* **5**, e22 (2008).
11. N. M. Fisk, M. McKee, R. Atun, Relative and absolute addressability of global disease burden in maternal and perinatal health by investment in R&D. *Trop. Med. Int. Health* **16**, 662–668 (2011).
12. W. Arap, R. Pasqualini, E. Ruoslahti, Cancer treatment by targeted drug delivery to tumor vasculature in a mouse model. *Science* **279**, 377–380 (1998).
13. E. Ruoslahti, S. N. Bhatia, M. J. Sailor, Targeting of drugs and nanoparticles to tumors. *J. Cell Biol.* **188**, 759–768 (2010).
14. D. Hanahan, J. Folkman, Patterns and emerging mechanisms of the angiogenic switch during tumorigenesis. *Cell* **86**, 353–364 (1996).
15. T. M. Allen, P. R. Cullis, Drug delivery systems: Entering the mainstream. *Science* **303**, 1818–1822 (2004).
16. E. Ruoslahti, Specialization of tumour vasculature. *Nat. Rev. Cancer* **2**, 83–90 (2002).
17. J. A. Hoffman, E. Giraudo, M. Singh, L. Zhang, M. Inoue, K. Porkka, D. Hanahan, E. Ruoslahti, Progressive vascular changes in a transgenic mouse model of squamous cell carcinoma. *Cancer Cell* **4**, 383–391 (2003).

18. L. Agemy, D. Friedmann-Morvinski, V. R. Kotamraju, L. Roth, K. N. Sugahara, O. M. Girard, R. F. Mattrey, I. M. Verma, E. Ruoslahti, Targeted nanoparticle enhanced proapoptotic peptide as potential therapy for glioblastoma. *Proc. Natl. Acad. Sci. U.S.A.* **108**, 17450–17455 (2011).
19. L. Agemy, V. R. Kotamraju, D. Friedmann-Morvinski, S. Sharma, K. N. Sugahara, E. Ruoslahti, Proapoptotic peptide-mediated cancer therapy targeted to cell surface p32. *Mol. Ther.* **21**, 2195–2204 (2013).
20. K. N. Sugahara, T. Teesalu, P. P. Karmali, V. R. Kotamraju, L. Agemy, O. M. Girard, D. Hanahan, R. F. Mattrey, E. Ruoslahti, Tissue-penetrating delivery of compounds and nanoparticles into tumors. *Cancer Cell* **16**, 510–520 (2009).
21. C. Ferretti, L. Bruni, V. Dangles-Marie, A. P. Pecking, D. Bellet, Molecular circuits shared by placental and cancer cells, and their implications in the proliferative, invasive and migratory capacities of trophoblasts. *Hum. Reprod. Update* **13**, 121–141 (2007).
22. R. Pijnenborg, L. Vercruysse, M. Hanssens, The uterine spiral arteries in human pregnancy: Facts and controversies. *Placenta* **27**, 939–958 (2006).
23. J.-H. Park, G. von Maltzahn, L. Zhang, M. P. Schwartz, E. Ruoslahti, S. N. Bhatia, M. J. Sailor, Magnetic iron oxide nanoworms for tumor targeting and imaging. *Adv. Mater.* **20**, 1630–1635 (2008).
24. L. Agemy, K. N. Sugahara, V. R. Kotamraju, K. Gujraty, O. M. Girard, Y. Kono, R. F. Mattrey, J.-H. Park, M. J. Sailor, A. I. Jimenez, C. Cativiela, D. Zanuy, F. J. Sayago, C. Aleman, R. Nussinov, E. Ruoslahti, Nanoparticle-induced vascular blockade in human prostate cancer. *Blood* **116**, 2847–2856 (2010).
25. M. Constância, M. Hemberger, J. Hughes, W. Dean, A. Ferguson-Smith, R. Fundele, F. Stewart, G. Kelsey, A. Fowden, C. Sibley, W. Reik, Placental-specific IGF-II is a major modulator of placental and fetal growth. *Nature* **417**, 945–948 (2002).
26. K. Forbes, M. Westwood, P. N. Baker, J. D. Aplin, Insulin-like growth factor I and II regulate the life cycle of trophoblast in the developing human placenta. *Am. J. Physiol. Cell Physiol.* **294**, C1313–C1322 (2008).
27. J. C. Charnock, M. R. Dilworth, J. D. Aplin, C. P. Sibley, M. Westwood, I. P. Crocker, The impact of a human IGF-II analogue ([Leu^{27}]IGF-II) on fetal growth in a mouse model of fetal growth restriction. *Am. J. Physiol. Endocrinol. Metab.* **310**, E24–E31 (2015).
28. K. Yamashita, Y. Yoshioka, K. Higashisaka, K. Mimura, Y. Morishita, M. Nozaki, T. Yoshida, T. Ogura, H. Nabeshi, K. Nagano, Y. Abe, H. Kamada, Y. Monobe, T. Imazawa, H. Aoshima, K. Shishido, Y. Kawai, T. Mayumi, S.-i. Tsunoda, N. Itoh, T. Yoshikawa, I. Yanagihara, S. Saito, Y. Tsutsumi, Silica and titanium dioxide nanoparticles cause pregnancy complications in mice. *Nat. Nanotechnol.* **6**, 321–328 (2011).
29. M. R. Dilworth, I. Andersson, L. J. Renshall, E. Cowley, P. Baker, S. Greenwood, C. P. Sibley, M. Wareing, Sildenafil citrate increases fetal weight in a mouse model of fetal growth restriction with a normal vascular phenotype. *PLOS One* **8**, e77748 (2013).
30. L. J. Renshall, M. R. Dilworth, S. L. Greenwood, C. P. Sibley, M. Wareing, In vitro assessment of mouse fetal abdominal aortic vascular function. *Am. J. Physiol. Regul. Integr. Comp. Physiol.* **307**, R746–R754 (2014).
31. A. N. Sferruzzi-Perri, J. A. Owens, K. G. Pringle, J. S. Robinson, C. T. Roberts, Maternal insulin-like growth factors-I and -II act via different pathways to promote fetal growth. *Endocrinology* **147**, 3344–3355 (2006).
32. A. E. Sutherland, P. G. Calarco, C. H. Damsky, Developmental regulation of integrin expression at the time of implantation in the mouse embryo. *Development* **119**, 1175–1186 (1993).
33. O. A. Vanderpuye, C. A. Labarrere, J. A. McIntyre, A vitronectin-receptor-related molecule in human placental brush border membranes. *Biochem. J.* **280**, 9–17 (1991).
34. Y. Zhou, S. J. Fisher, M. Janatpour, O. Genbacev, E. Dejana, M. Wheelock, C. H. Damsky, Human cytotrophoblasts adopt a vascular phenotype as they differentiate. A strategy for successful endovascular invasion? *J. Clin. Invest.* **99**, 2139–2151 (1997).
35. V. Fogal, L. Zhang, S. Krajewski, E. Ruoslahti, Mitochondrial/cell-surface protein p32/gC1qR as a molecular target in tumor cells and tumor stroma. *Cancer Res.* **68**, 7210–7218 (2008).
36. P. Matos, J. A. Horn, F. Beards, S. Lui, M. Desforges, L. K. Harris, A role for the mitochondrial-associated protein p32 in regulation of trophoblast proliferation. *Mol. Hum. Reprod.* **20**, 745–755 (2014).
37. D. M. Waisman, B. P. Salimath, M. J. Anderson, Isolation and characterization of CAB-63, a novel calcium-binding protein. *J. Biol. Chem.* **260**, 1652–1660 (1985).
38. M. Michalak, J. Groenendyk, E. Szabo, L. I. Gold, M. Opas, Calreticulin, a multi-process calcium-buffering chaperone of the endoplasmic reticulum. *Biochem. J.* **417**, 651–666 (2009).
39. M. G. Coppolino, M. J. Woodside, N. Demaurex, S. Grinstein, R. St-Arnaud, S. Dedhar, Calreticulin is essential for integrin-mediated calcium signalling and cell adhesion. *Nature* **386**, 843–847 (1997).
40. M. Obeid, A. Tesniere, F. Ghiringhelli, G. M. Fimia, L. Apetoh, J.-L. Perfettini, M. Castedo, G. Mignot, T. Panaretakis, N. Casares, D. Métivier, N. Larochette, P. van Endert, F. Ciccosanti, M. Piacentini, L. Zitvogel, G. Kroemer, Calreticulin exposure dictates the immunogenicity of cancer cell death. *Nat. Med.* **13**, 54–61 (2007).
41. L. Senovilla, I. Vitale, I. Martins, M. Tailler, C. Pailleret, M. Michaud, L. Galluzzi, S. Adjemian, O. Kepp, M. Niso-Santano, S. Shen, G. Mariño, A. Criollo, A. Boilève, B. Job, S. Ladoire, F. Ghiringhelli, A. Sistigu, T. Yamazaki, S. Rello-Varona, C. Locher, V. Poirier-Colame, M. Talbot, A. Valent, F. Berardinelli, A. Antoccia, F. Ciccosanti, G. M. Fimia, M. Piacentini, A. Fueyo, N. L. Messina, M. Li, C. J. Chan, V. Sigl, G. Pourcher, C. Ruckenstuhl, D. Carmona-Gutierrez, V. Lazar, J. M. Penninger, F. Madeo, C. López-Otín, M. J. Smyth, L. Zitvogel, M. Castedo, G. Kroemer, An immunosurveillance mechanism controls cancer cell ploidy. *Science* **337**, 1678–1684 (2012).
42. K. Burns, B. Duggan, E. A. Atkinson, K. S. Famulski, M. Nemer, R. C. Bleackley, M. Michalak, Modulation of gene expression by calreticulin binding to the glucocorticoid receptor. *Nature* **367**, 476–480 (1994).
43. W.-F. Chiang, T.-Z. Hwang, T.-C. Hour, L.-H. Wang, C.-C. Chiu, H.-R. Chen, Y.-J. Wu, C.-C. Wang, L.-F. Wang, C.-Y. Chien, J.-H. Chen, C.-T. Hsu, J. Y.-F. Chen, Calreticulin, an endoplasmic reticulum-resident protein, is highly expressed and essential for cell proliferation and migration in oral squamous cell carcinoma. *Oral Oncol.* **49**, 534–541 (2013).
44. Z. Shi, W. Hou, X. Hua, X. Zhang, X. Liu, X. Wang, Overexpression of calreticulin in pre-eclamptic placentas: Effect on apoptosis, cell invasion and severity of pre-eclampsia. *Cell Biochem. Biophys.* **63**, 183–189 (2012).
45. T. Teesalu, K. N. Sugahara, V. R. Kotamraju, E. Ruoslahti, C-end rule peptides mediate neuropilin-1-dependent cell, vascular, and tissue penetration. *Proc. Natl. Acad. Sci. U.S.A.* **106**, 16157–16162 (2009).
46. T. Teesalu, K. N. Sugahara, E. Ruoslahti, Mapping of vascular ZIP codes by phage display. *Methods Enzymol.* **503**, 35–56 (2012).
47. J.-H. Park, G. von Maltzahn, L. Zhang, A. M. Derfus, D. Simberg, T. J. Harris, E. Ruoslahti, S. N. Bhatia, M. J. Sailor, Systematic surface engineering of magnetic nanoworms for in vivo tumor targeting. *Small* **5**, 694–700 (2009).
48. L. K. Harris, I. P. Crocker, P. N. Baker, J. D. Aplin, M. Westwood, IGF2 actions on trophoblast in human placenta are regulated by the insulin-like growth factor 2 receptor, which can function as both a signaling and clearance receptor. *Biol. Reprod.* **84**, 440–446 (2011).
49. H. A. Lacey, T. Nolan, S. L. Greenwood, J. D. Glazier, C. P. Sibley, Gestational profile of Na^+/H^+ exchanger and Cl^-/HCO_3^- anion exchanger mRNA expression in placenta using real-time QPCR. *Placenta* **26**, 93–98 (2005).
50. X. Yue, H. Wang, F. Zhao, S. Liu, J. Wu, W. Ren, Y. Zhu, Hepatitis B virus-induced calreticulin protein is involved in IFN resistance. *J. Immunol.* **189**, 279–286 (2012).
51. J. D. Glazier, C. J. P. Jones, C. P. Sibley, Purification and Na^+ uptake by human placental microvillus membrane vesicles prepared by three different methods. *Biochim. Biophys. Acta* **945**, 127–134 (1988).
52. M. R. Dilworth, L. C. Kusinski, E. Cowley, B. S. Ward, S. M. Husain, M. Constância, C. P. Sibley, J. D. Glazier, Placental-specific *Igf2* knockout mice exhibit hypocalcemia and adaptive changes in placental calcium transport. *Proc. Natl. Acad. Sci. U.S.A.* **107**, 3894–3899 (2010).
53. M. R. Dilworth, L. C. Kusinski, B. C. Baker, L. J. Renshall, S. L. Greenwood, C. P. Sibley, M. Wareing, Defining fetal growth restriction in mice: A standardized and clinically relevant approach. *Placenta* **32**, 914–916 (2011).

Acknowledgments: We thank the research midwives of St. Mary's Hospital for their assistance in obtaining the placentas, F. Beards and J. Horn for excellent technical assistance, E. Engvall for comments on the manuscript, and the proteomics facility at the Sanford-Burnham Medical Research Institute for performing MALDI-TOF mass spectrometry. **Funding:** This research was funded by a Biotechnology and Biological Sciences Research Council David Phillips Fellowship (BB/H022627/1; to L.K.H.) and by the U.S. National Cancer Institute (R01 CA 152327; to E.R.). The Maternal and Fetal Health Research Centre is supported by funding from Tommy's the Baby Charity, an Action Research Endowment Fund, the Manchester Biomedical Research Centre, and the Greater Manchester Comprehensive Local Research Network. **Author contributions**: L.A., T.T., J.D.A., J.D.G., F.C., N.T., E.R., and L.K.H. designed the experiments; A.K., C.N., S.L., K.W., and L.K.H. performed the research; L.A. and V.R.K. contributed reagents; A.K., C.N., S.L., and L.K.H. analyzed the data; L.K.H. wrote the manuscript. All authors discussed the results and commented on the manuscript. **Competing interests:** The authors declare that they have no competing interests. **Data and materials availability:** A material transfer agreement exists between L.K.H. and E.R., permitting the use of homing peptides discovered in E.R.'s laboratory for use in creating platforms for targeted delivery of therapeutics to the placenta in L.K.H.'s laboratory. All data needed to evaluate the conclusions in the paper are present in the paper and/or the Supplementary Materials. Additional data related to this paper may be requested from the authors.

Submitted 18 February 2016
Accepted 8 April 2016
Published 6 May 2016
10.1126/sciadv.1600349

Citation: A. King, C. Ndifon, S. Lui, K. Widdows, V. R. Kotamraju, L. Agemy, T. Teesalu, J. D. Glazier, F. Cellesi, N. Tirelli, J. D. Aplin, E. Ruoslahti, L. K. Harris, Tumor-homing peptides as tools for targeted delivery of payloads to the placenta. *Sci. Adv.* **2**, e1600349 (2016).

ScienceAdvances
AAAS

Tumor-homing peptides as tools for targeted delivery of payloads to the placenta

Anna King, Cornelia Ndifon, Sylvia Lui, Kate Widdows, Venkata R. Kotamraju, Lilach Agemy, Tambet Teesalu, Jocelyn D. Glazier, Francesco Cellesi, Nicola Tirelli, John D. Aplin, Erkki Ruoslahti and Lynda K. Harris (May 6, 2016)
Sci Adv 2016, 2:.
doi: 10.1126/sciadv.1600349